CHEMISTRY OF MATERIALS
Cite This: Chem. Mater. 2017, 29, 10496−10509
Article
pubs.acs.org/cm

Order−Disorder Transitions and Superionic Conductivity in the Sodium *nido*-Undeca(carba)borates

Wan Si Tang,*[,†,‡] Mirjana Dimitrievska,*[,†,⊥] Vitalie Stavila,*[,§] Wei Zhou,[†] Hui Wu,[†] A. Alec Talin,[¶] and Terrence J. Udovic[†]

[†]NIST Center for Neutron Research, National Institute of Standards and Technology, Gaithersburg, Maryland 20899-6102, United States
[‡]Department of Materials Science and Engineering, University of Maryland, College Park, Maryland 20742-2115, United States
[⊥]National Renewable Energy Laboratory, Golden, Colorado 80401, United States
[§]Energy Nanomaterials, Sandia National Laboratories, Livermore, California 94551, United States
[¶]Materials Physics Department, Sandia National Laboratories, Livermore, California 94551, United States

Supporting Information

ABSTRACT: The salt compounds $NaB_{11}H_{14}$, Na-7-$CB_{10}H_{13}$, Li-7-$CB_{10}H_{13}$, Na-7,8-$C_2B_9H_{12}$, and Na-7,9-$C_2B_9H_{12}$ all contain geometrically similar, monocharged, *nido*-undeca(carba)borate anions (i.e., truncated icosohedral-shaped clusters constructed of only 11 instead of 12 {B−H} + {C−H} vertices and an additional number of compensating bridging and/or terminal H atoms). We used first-principles calculations, X-ray powder diffraction, differential scanning calorimetry, neutron vibrational spectroscopy, neutron elastic-scattering fixed-window scans, quasielastic neutron scattering, and electrochemical impedance measurements to investigate their structures, bonding potentials, phase-transition behaviors, anion orientational mobilities, and ionic conductivities compared to those of their *closo*-poly(carba)borate cousins. All exhibited order−disorder phase transitions somewhere between room temperature and 375 K. All disordered phases appear to possess highly reorientationally mobile anions (> ~10^{10} jumps s^{-1} above 300 K) and cation-vacancy-rich, close-packed or body-center-cubic-packed structures [like previously investigated *closo*-poly(carba)borates]. Moreover, all disordered phases display superionic conductivities but with generally somewhat lower values compared to those for the related sodium and lithium salts with similar monocharged 1-$CB_9H_{10}^-$ and $CB_{11}H_{12}^-$ *closo*-carbaborate anions. This study significantly expands the known toolkit of solid-state, poly(carba)borate-based salts capable of superionic conductivities and provides valuable insights into the effect of crystal lattice, unit cell volume, number of carbon atoms incorporated into the anion, and charge polarization on ionic conductivity.

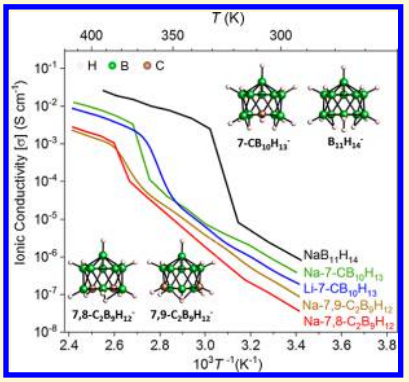

INTRODUCTION

Use of inorganic solid electrolytes in future lithium- or sodium-ion all-solid-state battery systems will, among other things, improve the energy density of the electrochemical cell and also improve safety by eliminating the flammable and hazardous liquid organic electrolyte.[1−3] However, one formidable requirement for solid electrolytes is to achieve ionic conductivity that is comparable to that of liquid electrolytes, e.g., σ_{Li^+} = 12 mS·cm^{-1} at room temperature (RT) for LP30 [1 M $LiPF_6$ (where M = mol·L^{-1}) in 1:1 ethylene carbonate:dimethyl carbonate (EC:DMC)][4] and σ_{Na^+} = 12 mS·cm^{-1} at RT for 1 M $NaClO_4$ in 1:1 EC:DMC.[5] Indeed, most solid electrolytes lack sufficient conductivity below 373 K.[1−3] Solid electrolytes with potentially promising RT ionic conductivities that have been more widely investigated in the past five years include (i) variants of chalcogen pnictides based on PS_4^{3-} (or PSe_4^{3-}) building blocks such as $Li_{10}GeP_2S_{12}$ (LGPS, σ_{Li^+} = 12 mS·cm^{-1}),[6] $Li_7P_3S_{11}$ (σ_{Li^+} = 17 mS·cm^{-1}),[7] $Li_{9.54}Si_{1.74}P_{1.44}S_{11.7}Cl_{0.3}$ (σ_{Li^+} = 25 mS·cm^{-1}),[8] and Na_3PSe_4 (σ_{Na^+} = 1.16 mS·cm^{-1});[9] (ii) Li garnet oxide ceramic materials (e.g., $Li_7La_3Zr_2O_{12}$, $\sigma_{Li^+} \approx$ 1 mS·cm^{-1});[10−12] and (iii) polymer/electrolyte composites (typically, σ_{Li^+} < 1 mS·cm^{-1}).[13,14] Despite their potentially acceptable ionic conductivities, all of these solid electrolytes suffer from various shortcomings such as an insufficiently wide electrochemical stability window; formation of reactive interfaces with either the anode, cathode, or both; and the inability to form low-resistance, conformal contacts to electrodes with complex morphologies.[15]

Due to these shortcomings, there is a need to explore alternative types of solid superionic conductors ($\sigma \approx$ 10 mS·cm^{-1}) with improved properties for room-temperature use.[16] Indeed, there has also been interest in finding sufficiently conductive solid electrolytes among the broad class of complex hydride-based compounds[17] such as the prototypical $LiBH_4$

Received: October 15, 2017
Revised: November 20, 2017
Published: November 20, 2017

DOI: 10.1021/acs.chemmater.7b04332
Chem. Mater. 2017, 29, 10496−10509

and $Na_2BH_4NH_2$ salts and related hybrid materials.[18−23] More recently, liquid-like ionic conductivity was discovered in borohydride materials based on relatively large, quasi-spherical, *closo*-polyborate and *closo*-polycarbaborate (i.e., $B_{12}H_{12}^{2-}$, $B_{10}H_{10}^{2-}$, $CB_{11}H_{12}^{-}$, and 1-$CB_9H_{10}^{-}$; see Figure 1) anion

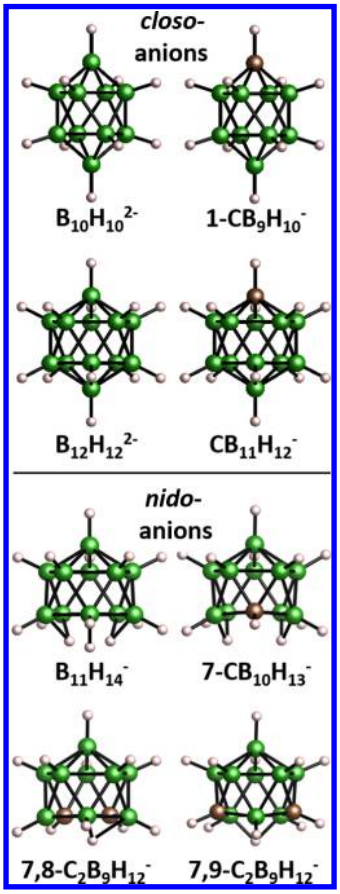

Figure 1. (top) *closo*-Poly(carba)borate anions that can form superionic conducting disordered salts with, e.g., Li^+ and Na^+ cations, and (bottom) geometrically related *nido*-poly(carba)borate anions explored in this study. White, green, and brown spheres denote H, B, and C atoms, respectively.

building blocks.[24−27] In the past decade, attention to *closo*-polyborate anions in particular has been focused on avoiding their undesirable formation as persistent side-products during the dehydrogenation of tetrahydroborate-containing hydrogen-storage materials[28−33] due to the stabilizing nature of the pseudoaromatic bonding.[34] Yet, as a component of a solid electrolyte, such high chemical (and electrochemical) stability is a desirable property. Indeed, a very recent computational study[35] confirms that, whereas Li and Na tetrahydroborate salts are unstable at high voltages, the corresponding *closo*-dodecaborates have wide electrochemical windows (up to 5 V). As a result, in contrast to the tetrahydroborate salts, polyhedral (carba)borate salts are typically air-stable at device-relevant temperatures as well as stable with respect to Li and Na metal anodes.

A relatively common characteristic of these *closo*-type salt compounds is the sudden jump in ionic conductivity above a phase-transition temperature (T_{trans}) as they change from an ordered low-T phase to an entropically driven, disordered high-T phase (type I superionic material).[16] For example, Na^+ conductivities attain superionic values of 0.1 S·cm^{-1} (at 540 K), 10 mS·cm^{-1} (at 383 K), 0.12 S·cm^{-1} (at 383 K), and 30 mS·cm^{-1} (at 297 K) for disordered body-centered-cubic (bcc) $Na_2B_{12}H_{12}$,[24] face-centered-cubic (fcc) $Na_2B_{10}H_{10}$,[25] fcc $NaCB_{11}H_{12}$,[26] and hexagonal Na-1-CB_9H_{10},[27] respectively; and Li^+ conductivities attain superionic values of 0.15 S·cm^{-1} (at 403 K) and 30 mS·cm^{-1} (at 354 K) for disordered fcc $LiCB_{11}H_{12}$ (ref 26) and hexagonal Li-1-CB_9H_{10},[27] respectively. This is similar to the ionic conductivity behavior observed in AgI, the first solid superionic conductor studied by Tubandt and Lorenz in 1914; the transition into the high-T α-AgI phase ($Im\bar{3}m$) above 420 K coincides with a rapid increase in conductivity (σ_{Ag^+} > 1.3 S·cm^{-1})[36] because the highly disordered nature of Ag^+ cations within the anionic bcc sublattice enabled liquid-like motion of the cations.[37,38] In the *closo*-type materials, the partially filled cationic Wyckoff sites in combination with the relatively large size and high orientational mobility of the *closo*-poly(carba)borate anions facilitate rapid diffusion of the cations through the disordered unit cell. Anion reorientational jump rates above 10^{10}−10^{11} s^{-1} are confirmed from quasielastic neutron scattering (QENS) and solid-state nuclear magnetic resonance (NMR) studies.[24,25,39−44] Ab initio molecular dynamics computations[35,45−47] strongly suggest that these highly mobile anions are indeed not just inconsequential bystanders during cation diffusion, but rather act as critical synergistic partners during cation translational jumps through the lattice, effectively lowering the cation diffusional barrier and enhancing the ultimate superionic conductivities observed.

It is worth noting that the anionic modification of the *closo*-polyborate anions ($B_{12}H_{12}^{2-}$ and $B_{10}H_{10}^{2-}$) to form *closo*-polycarbaborate anions ($CB_{11}H_{12}^{-}$ and 1-$CB_9H_{10}^{-}$) by replacing one {B−H} vertex with {C−H} on an apical site leads to a unit reduction in negative charge. Hence, *closo*-polycarbaborate salts possess half as many cations as *closo*-polyborate salts to maintain charge neutrality, which may allow for better cationic movement within the unit cell, due to decreased cation-site blockage, reduced anion−cation Coulombic interactions, and more orientationally mobile anions.[26,27,44] Indeed, the conductivity values associated with disordered *closo*-polycarbaborate salts with singly charged anions measured thus far seem to be about an order of magnitude higher than those of their *closo*-polyborate analogues at similar temperatures.[26,27] Moreover, there are indications that disordered Na polycarbaborate salts are at least as good if not better conductors than their Li polycarbaborate congeners.[26,27]

Various other *closo*-type compound modifications have been explored in an effort to stabilize the desired superionic disordered phase to lower temperatures as well as to further enhance the superionic conductivity. Attempted cationic modifications such as the replacement of some Li^+ with Na^+ to form $Li_{2-y}Na_yB_{12}H_{12}$ (with y = 0.67, 1.00, and 1.33) yielded T_{trans} values intermediate between those of pure $Na_2B_{12}H_{12}$ and $Li_2B_{12}H_{12}$.[48] $Na_2B_{12}X_{12}$ compounds with halogenated $B_{12}X_{12}^{2-}$ anions (X = F, Cl, Br, I) yielded T_{trans} values even higher than that for $Na_2B_{12}H_{12}$.[48−50]

One successful strategy for further stabilizing superionic disordered phases at and below RT has involved crystallite-size reduction via ball-milling. For example, ball-milled $Li_2B_{12}H_{12}$ and $Na_2B_{12}H_{12}$ showed enhanced ionic conductivities of 10^{-3} S·cm^{-1} at 423 and 323 K, respectively.[51] Another successful strategy has involved synthesis of mixed *closo*-poly(carba)-borate-anion solid-solution phases such as $Na_4(B_{12}H_{12})$-$(B_{10}H_{10})$, $Na_2(1\text{-}CB_9H_{10})(CB_{11}H_{12})$, $Li_2(1\text{-}CB_9H_{10})(CB_{11}H_{12})$, and $B_{12}H_{12-x}I_x$-doped $Na_2B_{12}H_{12}$.[51−55] Indeed, the highest

DOI: 10.1021/acs.chemmater.7b04332
Chem. Mater. 2017, 29, 10496−10509

solid-state Na^+ conductivity to date, exceeding 0.1 S cm^{-1} at RT, was reported for a $Na_2(1\text{-}CB_9H_{10})(CB_{11}H_{12})$ solid-solution phase formed by ball-milling a 1:1 $Na\text{-}1\text{-}CB_9H_{10}$:$NaCB_{11}H_{12}$ mixture.[52] In these strategies, nanosizing and anion geometric stacking frustration are both thought to promote the stabilization of the desirable HT-like disordered phases down to subambient temperatures. Moreover, some *closo*-polyborate synthesis methods naturally result in mixed-anion phases that can potentially lead to desirable superionically conductive disordered materials.[52,56−59] Finally, there has also been some success with making RT fast-ion conductors such as $Na_3(BH_4)(B_{12}H_{12})$, $Ag_{2+x}I_xB_{12}H_{12}$, and $Ag_{2+x}I_xB_{10}H_{10}$ by mixing *closo*-type anions with non-*closo*-type anions.[60,61]

On the basis of the highly favorable conductivity properties of the *closo*-type compounds as solid electrolytes, we extended our investigations to include a related type of anion-modified compound, namely, the *nido*-poly(carba)borates. (NB, *closo* and *nido* mean cage and nest, respectively, from the Greek). Within this broad family of cluster *nido*-compounds, we focused our attention herein mainly on the sodium salts of the following *nido*-poly(carba)borate anions (see Figure 1): (i) tetradecahydro-*nido*-undecaborate(−) ($B_{11}H_{14}^-$), (ii) di-μ-hydro-undecahydro-7-monocarba-*nido*-undecaborate(−) ($7\text{-}CB_{10}H_{13}^-$), (iii) dodecahydro-7,8-dicarba-*nido*-undecaborate(−) ($7,8\text{-}C_2B_9H_{12}^-$), and (iv) dodecahydro-7,9-dicarba-*nido*-undecaborate(−) ($7,9\text{-}C_2B_9H_{12}^-$). For all these anions, the nest-like *nido*-structure is similar to the cage-like *closo*-structure but truncated with one icosohedral cage atom completely removed. Hence, instead of the usual 12 vertices (e.g., $B_{12}H_{12}^{2-}$or $CB_{11}H_{12}^-$), there are only 11 in the featured compounds.[62] Yet, this is different from a typical *closo*-$B_{11}H_{11}^-$ structure[63,64] because the icosahedral skeleton based on 12 vertices is still preserved. Figure 1 compares the various *closo*- and *nido*-structures, and Figures S1−S4 in the Supporting Information further highlight the standard numbering of the atoms in the $B_{11}H_{14}^-$, $7\text{-}CB_{10}H_{13}^-$, $7,8\text{-}C_2B_9H_{12}^-$, and $7,9\text{-}C_2B_9H_{12}^-$ *nido*-anions by the International Union of Pure and Applied Chemistry (IUPAC). All of the *nido*-anions described here are singly charged clusters with some B/C nest-edge atoms bonded to more than one hydrogen. The extra hydrogen(s) bonded to these B/C atoms can either be a second endohydrogen or a bridging hydrogen (B−H−B bond).

In the structure of $B_{11}H_{14}^-$ and those of the other studied *nido*-anions, at least one hydrogen atom is bonded to each of the 11 B(C) cage atoms. It was initially thought that the three additional H atoms in $B_{11}H_{14}^-$ were unbonded to any B atoms and were rather described as an H_3^+ triangle interacting with a $B_{11}H_{11}^{2-}$ fragment on the open side of the dodecahedron.[65,66] However, with NMR and modeling, it is now widely accepted that two of the three are bridging H atoms, forming B−H−B bonds between B7−B8 and B10−B11, and the third is an endohydrogen bonded to B9[67−70] (see Figure S1). Various alkali salt solutions have been synthesized as precursors, but the crystals were not dried for structural characterization.[67]

In the structure of the most common *nido*-$CB_{10}H_{13}$ anion isomer, $7\text{-}CB_{10}H_{13}^-$, both hydrogens (di-μ-hydro-) form bridging B−H−B bonds between B8−B9 and B10−B11 on the lower equatorial positions of the *nido*-anion[71,72] (see Figure S2). $Cs\text{-}7\text{-}CB_{10}H_{13}$ was previously explored as a potential solid ionic conductor, showing two polymorphs over a transition temperature range of 437−470 K.[72] Both α- and β-phases were found to be monoclinic, with the structure of the α-polymorph completely solved. With this observed structural behavior, the authors concluded that no appreciable ionic conductivity was expected. There are two other possible *nido*-$CB_{10}H_{13}^-$ anion isomers, $1\text{-}CB_{10}H_{13}^-$ and $2\text{-}CB_{10}H_{13}^-$, but neither of these are considered further here.

The two most common isomeric *nido*-$C_2B_9H_{12}^-$ anions ($7,8\text{-}C_2B_9H_{12}^-$ and $7,9\text{-}C_2B_9H_{12}^-$) each contain two carbon atoms in the lower equatorial positions of the skeletal framework. The carbons are found either next to each other ($7,8\text{-}C_2B_9H_{12}^-$) or separated by a B atom ($7,9\text{-}C_2B_9H_{12}^-$), and this leads to differences in packing and structure. One main distinction is the position of the twelfth or last hydrogen, which is not singly bonded to one boron/carbon and remained unresolved in both structures for a long time after their discovery. It has since been determined to be a B−H−B bridging hydrogen in both anions.[73−75] From powder X-ray and neutron diffraction studies of the 7,8-*nido*-dicarbaborate anion, an asymmetric B−H−B bridge was found over the B10−B11 bond[73,74] instead of fluctuating between B9−B10 and B10−B11 (see Figure S3). In the 7,9-isomer, the bridging hydrogen was clearly found between the B10−B11 bond[75] (see Figure S4). It is interesting to note that the "extra" hydrogen is not bonded to the more electropositive carbon in the anion, i.e. there is no presence of C−H−C or B−H−C bonds. $Cs\text{-}7,8\text{-}C_2B_9H_{12}$ was previously investigated as a possible solid ionic conductor, showing two phase changes from a monoclinic γ-phase to a monoclinic (pseudo-orthorhombic) β-phase (at 374 K) to a disordered tetragonal α-phase (at 483 K).[76] The predominant migration of the Cs^+ cations along the *c*-axis of the α-polymorph was believed to be responsible for the observed conductivity (σ_{Cs^+} = 55 μS·cm^{-1} at 478 K). There are seven other possible *nido*-$C_2B_9H_{12}^-$ anion isomers such as $1,2\text{-}C_2B_9H_{12}^-$ and $1,7\text{-}C_2B_9H_{12}^-$, but none of these are considered further here.

Here, we present the properties of the sodium salts of the aforementioned *nido*-undeca(carba)borate anions (i.e., $NaB_{11}H_{14}$, $Na\text{-}7\text{-}CB_{10}H_{13}$, $Na\text{-}7,8\text{-}C_2B_9H_{12}$, and $Na\text{-}7,9\text{-}C_2B_9H_{12}$), as well as one comparative lithium salt analogue, $Li\text{-}7\text{-}CB_{10}H_{13}$, as determined by a variety of techniques: differential scanning calorimetry (DSC), X-ray powder diffraction (XRPD), neutron vibrational spectroscopy (NVS), neutron-elastic-scattering fixed-window-scans (FWS), quasielastic neutron scattering (QENS), and AC impedance. These *nido*-compounds are also found to form superionic disordered structures like their *closo*-type cousins. Moreover, one of the two different batches of commercially available $NaB_{11}H_{14}$ investigated displayed no obvious order−disorder phase transition. Rather, it maintained a persistent and highly conductive disordered structure down to subambient temperatures, atypical behavior that was previously observed in related *closo*-polyborate salts containing some minor amount of substitutional anion impurities.

EXPERIMENTAL DETAILS

Sodium *nido*-undecaborate, $NaB_{11}H_{14}$ (two different batches); the sodium and lithium monocarba-*nido*-undecaborates, $Na\text{-}7\text{-}CB_{10}H_{13}$ and $Li\text{-}7\text{-}CB_{10}H_{13}$; and the sodium dicarba-*nido*-undecaborates, $Na\text{-}7,8\text{-}C_2B_9H_{12}$ and $Na\text{-}7,9\text{-}C_2B_9H_{12}$, were all obtained from Katchem.[77] Removal of any residual water was typically accomplished by annealing for 16 h under vacuum at 373 K for $NaB_{11}H_{14}$ and at 393 K for all other *nido*-compounds. In addition, sodium decahydro-*closo*-deca(carba)borates $Na\text{-}1\text{-}CB_9H_{10}$ and $Na_2B_{10}H_{10}$ were also used in this study as ionic conductivity reference materials, and sodium monocarba-*closo*-dodecaborate, $NaCB_{11}H_{12}$, was used both as an additional ionic conductivity reference material and for comparative anion reorientational mobility measurements. $Na\text{-}1\text{-}CB_9H_{10}$ and

DOI: 10.1021/acs.chemmater.7b04332
Chem. Mater. 2017, 29, 10496−10509

$NaCB_{11}H_{12}$ were obtained from Katchem. $Na_2B_{10}H_{10}$ was made by an ion-exchange method similar to that in ref 25, starting with $(NH_4)_2B_{10}H_{10}$ from Katchem. All three samples were dried for about 16 h under vacuum at 473 K.

XRPD patterns were measured for each sample sealed in quartz capillaries at RT and above using a Rigaku Ultima III X-ray diffractometer with a Cu Kα source (λ = 1.5418 Å). Elevated sample temperatures were enabled by a calibrated radiative/convective heat source. XRPD structural refinements were performed using either GSAS[78] or Fullprof software.[79] Differential scanning calorimetry measurements were made with a Netzsch (STA 449 F1 Jupiter) TGA-DSC under He flow using Al sample pans.

All neutron scattering experiments were performed at the National Institute of Standards and Technology Center for Neutron Research. NVS measurements at 4 K were done on the filter-analyzer neutron spectrometer (FANS)[80] using the Cu(220) monochromator with pre- and postcollimations of 20′ of arc, yielding a full width at half-maximum (fwhm) energy resolution of about 3% of the neutron energy transfer. QENS measurements for $NaB_{11}H_{14}$ up to 410 K and $NaCB_{11}H_{12}$ up to 480 K were done on the disc chopper spectrometer (DCS),[81] utilizing an incident neutron wavelength of 8 Å (1.28 meV) with a resolution of 30 μeV fwhm and a maximum attainable neutron momentum transfer (Q) value of around 1.48 $Å^{-1}$. The lowest $NaB_{11}H_{14}$ dynamical measurement at 310 K utilized a wavelength of 10 Å (0.818 meV) with a resolution of 17 μeV fwhm and a maximum attainable Q value of around 1.18 $Å^{-1}$. The resolution functions for both wavelengths were obtained from the purely elastic 30 K QENS measurements. Because all samples were synthesized with natural boron, which contains the highly neutron-absorbing ^{10}B isotope, thin flat-plate sample geometries were used for FANS and DCS measurements, and all scattering was done in reflection. Neutron-elastic-scattering fixed-window scans (FWSs) between 120 and 430 K were done for all *nido*-compounds on the high-flux backscattering spectrometer (HFBS),[82] which provides a resolution of 0.8 μeV fwhm using 6.27 Å wavelength incident neutrons. Again, very thin, flat-plate-shaped samples were used to minimize neutron beam attenuation from the presence of ^{10}B. All neutron data analyses were done with the DAVE software package.[83]

AC impedance measurements were performed inside an Ar-filled glovebox. The electrolyte powders were pressed into free-standing pellets with a diameter of 6.35 mm and thicknesses that ranged from 2.7 to 3.4 mm. The pellets were formed under 250 MPa uniaxial pressure using a Carver hydraulic press and loaded into an MTI stainless steel cell with Au electrodes on both sides of the pellet. The measurements were performed at temperatures from room temperature to 415 K for all compounds except for $NaB_{11}H_{14}$, which was measured down to 255 K. The sample temperature was measured using a calibrated thermocouple. The AC impedance spectra were collected from 0.1 Hz to 1 MHz using a Gamry600 potentiostat, and the data were analyzed using Gamry software to extract the electrolyte resistance.

To complement the structural refinements and NVS measurements, first-principles calculations were performed within the plane-wave implementation of the generalized gradient approximation to density functional theory (DFT) using a Vanderbilt-type ultrasoft potential with Perdew–Burke–Ernzerhof exchange correlation.[84] A cutoff energy of 544 eV and a 2 × 2 × 2 k-point mesh (generated using the Monkhorst–Pack scheme) were used and found to be enough for the total energy to converge within 0.01 meV/atom. For comparison with the NVS measurements, the phonon density of states (PDOS) was calculated for the DFT-optimized 0 K ordered structures (except for $NaB_{11}H_{14}$ and Li-7-$CB_{10}H_{13}$) using the supercell method with finite displacements[85,86] and were appropriately weighted to take into account the H, Na, B, and C total neutron scattering cross sections. Mulliken atomic charges associated with the isolated $B_{11}H_{14}^-$, 7-$CB_{10}H_{13}^-$, 7,8-$CB_9H_{12}^-$, and 7,9-$CB_9H_{12}^-$ anions were also determined from DFT calculations of the energy-optimized anion geometries using 20 × 20 × 20 supercells.

All structural depictions were made using the VESTA (visualization for electronic and structural analysis) software.[87] For all figures, standard uncertainties are commensurate with the observed scatter in the data, if not explicitly designated by vertical error bars

RESULTS AND DISCUSSION

1. Phase-Transition Behaviors: DSC. Differential scanning calorimetry was initially used to locate potential phase transitions for the various *nido*-compounds. Figure 2 illustrates

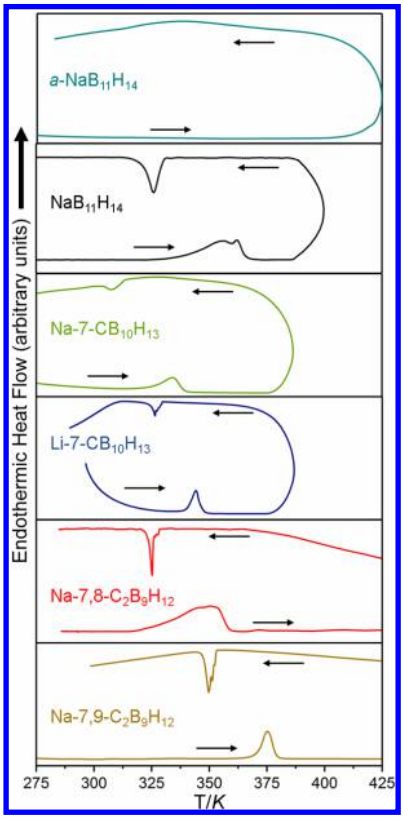

Figure 2. DSC plots for all *nido*-compounds in heating and cooling at ±20 K s^{-1}.

the characteristic DSC scans upon heating and cooling. For each compound, there is a clear endothermic feature upon heating and a matching hysteretic exothermic feature upon cooling somewhere within a 300 to 375 K temperature range, which are presumed to mark the presence of reversible order–disorder phase transitions. For $NaB_{11}H_{14}$, the first of two purchased batches lacked any similar calorimetric features between 225 and 425 K, as seen by the top plot in Figure 2, suggesting that no phase change occurred for this particular atypical $NaB_{11}H_{14}$ sample (which for brevity, we will from here on refer to as *a*-$NaB_{11}H_{14}$), at least within this range. This anomalous behavior prompted us to purchase a second separately synthesized batch, which in turn demonstrated a clear hysteretic phase-change behavior more in line with the other *nido*-compounds measured. Both $NaB_{11}H_{14}$ samples were found to possess similar thermal stabilities, being slightly less robust than the other *nido*-compounds studied (we note that, because of the intriguing variations found in structural and dynamical properties between both $NaB_{11}H_{14}$ samples, we compare their various properties throughout this paper). For all *nido*-compounds measured, the onset of decomposition (with mass loss) seemed to occur noticeably above around 450 K, although for $NaB_{11}H_{14}$, very slow decomposition may occur

DOI: 10.1021/acs.chemmater.7b04332
Chem. Mater. 2017, 29, 10496–10509

Table 1. Phase-Transition Temperatures Determined from DSC and Structural Symmetries of the Ordered and Disordered Phases Determined from XRPD

nido-compound	DSC T_{trans} (K) (heating)	DSC T_{trans} (K) (cooling)	symmetry of RT ordered structure	symmetry of HT disordered structure
a-$NaB_{11}H_{14}$				*Fm*-3*m* (fcc)/298 K *a* = 10.1520(19) Å *V* = 1046.3(3) Å^3
$NaB_{11}H_{14}$	353, 361	326	*Pnma* (orthorhombic) *a* = 10.9415(9) Å *b* = 7.5365(8) Å *c* = 12.1031(11) Å *V* = 998.03(26) Å^3 +minor fcc phase *a* = 9.998(6) Å *V* = 999.4(18) Å^3	*I*-43*d* (bcc)/350 K *a* = 15.922(5) Å *V* = 4037(4) Å^3 +minor fcc phase
Na-7-$CB_{10}H_{13}$	333	305	*Pna*2$_1$ (orthorhombic) *a* = 10.9919(4) Å *b* = 11.6564(5) Å *c* = 7.1720(4) Å *V* = 918.91(7) Å^3	*Fm*-3*m* (fcc)/370 K *a* = 9.983(2) Å *V* = 994.9(4) Å^3
Li-7-$CB_{10}H_{13}$	340	327	*P*2$_1$/*n* (monoclinic) *a* = 6.8263(14) Å *b* = 9.6314(16) Å *c* = 5.9391(13) Å *β* = 92.93(6) ° *V* = 389.96(13) Å^3	*Aea*2 (orthorhombic)/370 K *a* = 11.271(2) Å *b* = 9.7634(14) Å *c* = 8.7479(15) Å *V* = 962.6(3) Å^3
Na-7,8-$C_2B_9H_{12}$	347, 366	326	*P*2$_1$ (monoclinic) *a* = 8.3918(8) Å *b* = 7.5754(5) Å *c* = 7.1810(5) Å *β* = 91.249(1) ° *V* = 456.39(6) Å^3	*P*31*c* (trigonal)/370 K *a* = 7.0126(12) Å *c* = 11.3800(19) Å *V* = 484.65(14) Å^3
Na-7,9-$C_2B_9H_{12}$	375	351, 349	*Pna*2$_1$ (orthorhombic) *a* = 10.8351(3) Å *b* = 11.8931(4) Å *c* = 6.8717(2) Å *V* = 885.51(5) Å^3	*Fm*-3*m* (fcc)/423 K *a* = 9.9379(20) Å *V* = 981.5(3) Å^3

over hours even by 400 K. Table 1 summarizes the approximate phase-change temperatures for each compound.

2. Structural Behaviors: XRPD. XRPD patterns of *a*-$NaB_{11}H_{14}$, $NaB_{11}H_{14}$, Na-7-$CB_{10}H_{13}$, Li-7-$CB_{10}H_{13}$, Na-7,8-$C_2B_9H_{12}$, and Na-7,9-$C_2B_9H_{12}$ were measured at RT and above their DSC transition temperatures and are shown in Figure 3. Except for *a*-$NaB_{11}H_{14}$, the XRPD patterns of all other *nido*-compounds change from those reflecting an ordered structure at RT, typically orthorhombic or monoclinic, to those reflecting disordered structures above their transition temperatures. The *a*-$NaB_{11}H_{14}$ maintains an fcc disordered structure, even at RT, and DSC data in Figure 2 suggest that this structure persists down to at least 225 K. At this point, we cannot pinpoint with certainty what causes this anomalous behavior for *a*-$NaB_{11}H_{14}$ because vendor information indicates a predominance of $B_{11}H_{14}^-$ anions are indeed present for both purchased batches. Yet, it is evident from an observable difference in unit cell volumes between *a*-$NaB_{11}H_{14}$ and $NaB_{11}H_{14}$ (see discussion below) that some type of minor impurities such as anion and/or cation substitutional impurities and/or even some trace solvent adduct is causing a slight cell expansion for the former. The presence of such impurities is known to stabilize disordered structures in related *closo*-compounds below their expected pristine-compound transition temperatures.[51−61]

Similar to that of *a*-$NaB_{11}H_{14}$, the disordered structures for Na-7-$CB_{10}H_{13}$, Li-7-$CB_{10}H_{13}$, and Na-7,9-$C_2B_9H_{12}$ appear to reflect cubic-close-packed arrangements of orientationally disordered anions with cation-vacancy-rich interstitial sublattices, analogous to the structural nature of most superionic *closo*-poly(carba)borate compounds above their transition temperatures.[25−27,50,52] Na-7,8-$C_2B_9H_{12}$ is found to be one exception, forming a hexagonal-close-packed arrangement of anions, another polymorph stacking seen for disordered *closo*-poly(carba)borate compounds.[26,27,52,55] $NaB_{11}H_{14}$ is found to be another exception, forming predominantly bcc disorder with only a very minor fraction of fcc polymorph, as observed for $Na_2B_{12}H_{12}$.[40] This is interesting because *a*-$NaB_{11}H_{14}$ clearly favors fcc disorder. As mentioned above, a comparison of fcc lattice constants for each $NaB_{11}H_{14}$ sample at RT suggests a slightly larger lattice constant by 1.5% for *a*-$NaB_{11}H_{14}$ (i.e., 10.1520(19) Å for the latter vs 9.998(6) Å) and provides a further clue that some impurities affecting unit cell size are indeed present. Of course, this can also explain the observed differences in the higher-temperature anion stackings because the favored disordered polymorph has been shown to be sensitive among other things to unit cell size.[55] Finally, although the 370 K Li-7-$CB_{10}H_{13}$ pattern also largely reflects cubic-close-packing of the anions, the positions of the small Bragg scattering features suggests orthorhombic symmetry. No

DOI: 10.1021/acs.chemmater.7b04332
Chem. Mater. 2017, 29, 10496−10509

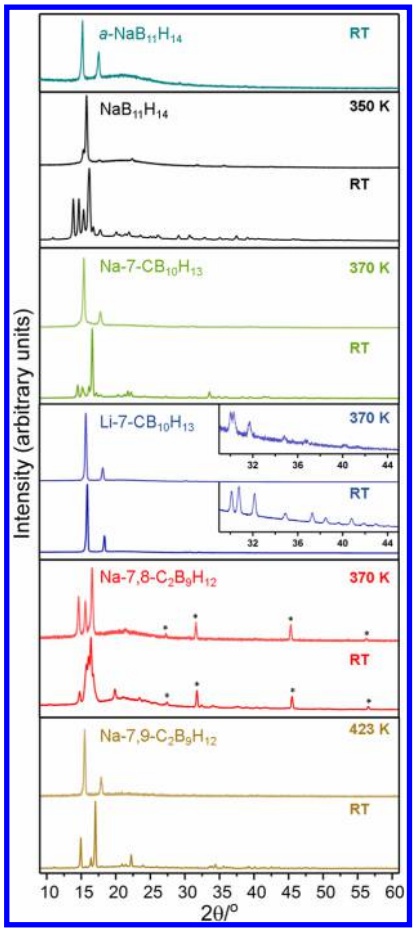

Figure 3. XRPD patterns for all *nido*-compounds both at RT and above their order−disorder phase-transition temperatures. The exception is *a*-$NaB_{11}H_{14}$, which is already fcc disordered at RT. Asterisks associated with the Na-7,8-$C_2B_9H_{12}$ patterns denote inadvertent NaCl contamination.

effort was made to determine if complete fcc symmetry was eventually attained at higher temperatures.

Table 1 summarizes the symmetries and unit cell parameters for the ordered and disordered phases of the various compounds. For two compounds, Na-7-$CB_{10}H_{13}$ and Na-7,9-$C_2B_9H_{12}$, the ordered RT structures were fully determined from Rietveld refinements, and these structures were confirmed as low-energy structures by DFT analyses. Figures S5−S9 in the Supporting Information depict more detailed XRPD results for these compounds, including Rietveld refinement fits of the patterns. For Na-7,8-$C_2B_9H_{12}$, we determined the most probable RT structure (see Figure S10) based on only partial success of refining a monoclinic structural model that fits the pattern, as some of the intensities of the smaller Bragg features were not in full agreement. This may be due to the presence of texturing or some unknown impurities and requires further investigation. Accompanying DFT analysis indicated that this was indeed a low-energy structure.

The detailed RT monoclinic structure of Li-7-$CB_{10}H_{13}$ (containing low-Z Li) remains unknown, and a solution may require complementary neutron powder diffraction measurements. As with all the other patterns shown in Figure 3, cell parameters and possible symmetry were determined by fitting the indexed peak positions. The Li-7-$CB_{10}H_{13}$ cell volumes/formula unit for both ordered and disordered phases appear to be smaller than those for Na-7-$CB_{10}H_{13}$, as expected from the relative cation sizes.

Rietveld refinement of the RT pattern for $NaB_{11}H_{14}$ (which we consider as representative of the pure compound) indicates that the structure is orthorhombic, but a reasonable agreement can only be found if one assumes that there is anion orientational disorder around the axis perpendicular to the plane defined by the five B nest atoms (see Figure S5). Thus, although the Na^+ cations appear to be ordered, the structure may actually be partially disordered with respect to the anions. We note that this orientational disorder model is not certain at this point because an additional fully ordered model that invokes large anisotropic B thermal factors could also be reconciled with the data. Additional detailed neutron powder diffraction measurements at lower temperatures may ultimately be required to verify the true structure and its temperature dependence.

Tables S1−S11 and additional CIF files for RT Na-7-$CB_{10}H_{13}$ and Na-7,9-$C_2B_9H_{12}$ in the Supporting Information summarize the various crystal structure parameters from the model fits of all the patterns in Figure 3. The XRPD results indicate two notable trends for the Na *nido*-compounds: (i) the unit cell volumes tend to decrease as the number of carbon atoms incorporated in each anion increases from 0 to 1 to 2, and (ii) the cations tend to avoid proximity to the more electropositive {C−H} vertices of the *nido*-polycarbaborate anions, similar to the behavior observed previously for the *closo*-compounds $LiCB_{11}H_{12}$, $NaCB_{11}H_{12}$, and Na-1-CB_9H_{10}.[26,88]

3. Bonding Interactions: NVS. The neutron vibrational spectra between 320 and 1330 cm^{-1} (1 meV ≈ 8.066 cm^{-1}) for *nido*-compounds at 4 K are shown in Figure 4 with comparisons possible in three cases (for Na-7-$CB_{10}H_{13}$, Na-7,8-$C_2B_9H_{12}$, and Na-7,9-$C_2B_9H_{12}$) to the calculated PDOSs for the 0 K, DFT-optimized, fully ordered structures derived from the RT XRPD data. In this region, the spectra are all dominated by various optical vibrational modes involving H atom displacements (in particular, anion deformation modes) due to the overwhelmingly large neutron scattering cross-section for H atoms compared to B, C, Na, or Li. They reflect the interatomic bonding interactions unique to each different anion as well as the bonding perturbations due to the various structure-dependent cation−anion and anion−anion interactions. We note that the hydrogen stretching modes are at higher energies outside the measured energy range. There is generally very good agreement between the experimental and simulated spectra, which corroborates the structures determined from XRPD. DFT simulations have previously indicated that neutron vibrational spectra of poly(carba)borate compounds are noticeably sensitive to the crystallographic structure details.[26,42,88−90] Further information about the natures of the different phonon modes contributing to the simulated PDOSs for the three Na polycarbaborate compounds can be provided by visualization software[91] using the ASCII .txt files in the Supporting Information.

For Li-7-$CB_{10}H_{13}$, where a detailed ordered structural model is lacking, the spectrum looks fairly similar to that for Na-7-$CB_{10}H_{13}$, suggesting similar local structural arrangements, although this must be verified by future PDOS calculations after the low-temperature Li-7-$CB_{10}H_{13}$ structure has been determined. Finally, we were only able to measure the 4 K FANS spectrum for *a*-$NaB_{11}H_{14}$ (and not $NaB_{11}H_{14}$) in the beamtime allotted to us. We also have no possible fully ordered structural model to use (based on the RT XRPD data for

DOI: 10.1021/acs.chemmater.7b04332
Chem. Mater. 2017, 29, 10496−10509

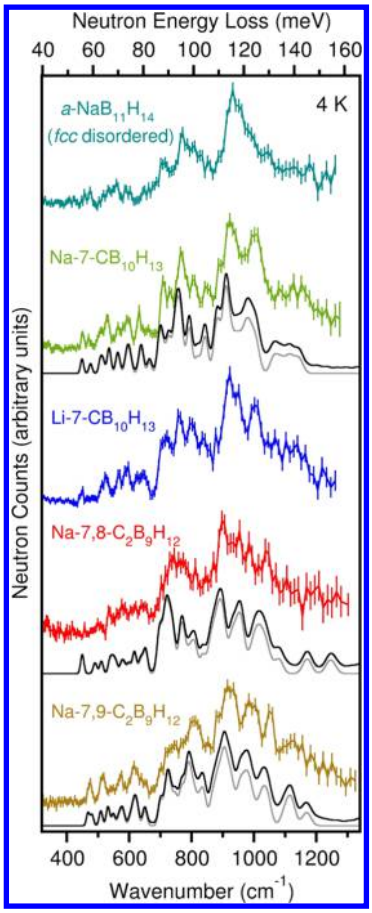

Figure 4. Neutron vibrational spectra for *nido*-compounds at 4 K (black) compared with the DFT-simulated phonon densities of states for the three Na *nido*-polycarbaborates after energy optimization of the XRPD-derived ordered RT structures [1-phonon DOS (gray) and 1 + 2-phonon DOS (black)]. NB, of the two $NaB_{11}H_{14}$ samples studied, only the (fcc disordered) *a*-$NaB_{11}H_{14}$ spectrum was measured.

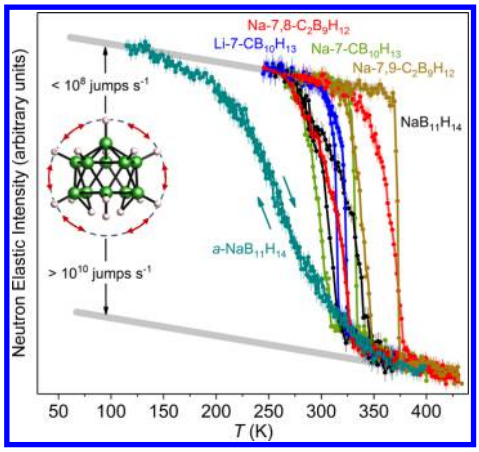

Figure 5. Neutron fixed-window scans for all *nido*-compounds during heating and cooling segments (denoted by arrows) at ±0.3 K min^{-1}. To improve the statistics of these natural-boron compounds, the data reflect summed intensities from detectors covering a *Q* range of 0.87–1.68 $Å^{-1}$. For a reasonable qualitative comparison, the individual data sets were scaled to have similar minimum and maximum intensities. Inset denotes the magnitudes of the fundamental reorientational jump frequencies for the *nido*-anions (schematically exemplified by $B_{11}H_{14}^-$) associated with the two asymptotic intensity plateaus at low and high temperatures.

pristine $NaB_{11}H_{14}$) to calculate a simulated PDOS for comparison to the 4 K *a*-$NaB_{11}H_{14}$ spectrum in Figure 4. Yet, this is probably moot because the 4 K *a*-$NaB_{11}H_{14}$ spectrum, although dominated by vibrations involving $B_{11}H_{14}^-$ anions, likely reflects the same highly disordered fcc structural arrangement observed by XRPD at RT. Neutron powder diffraction patterns extracted from our QENS measurements of *a*-$NaB_{11}H_{14}$ (discussed later in this paper) confirmed that the fcc disordered phase persists down to at least 30 K, the lowest temperature studied.

4. Anion Orientational Mobilities: FWSs and QENS. Changes in the anion orientational mobilities for the various *nido*-compounds upon thermal cycling through the reversible phase transitions were reflected by the neutron-elastic-scattering FWSs in Figure 5. All FWSs were dominated by the scattering from the bonded H atoms associated with the anions again due to hydrogen's overwhelmingly large neutron scattering cross-section compared to those for B, C, Na, or Li. In an FWS, the elastic (i.e., at zero energy transfer) scattering intensity is recorded while ramping the sample temperature in either a positive (heating) or negative (cooling) direction. Within the 0.8 μeV fwhm HFBS resolution window, the neutrons are typically able to sense H (and thus anion) reorientational jump frequencies above about 10^8 s^{-1}. Hence, in a typical FWS starting at the lowest temperatures where the H atoms are jumping less than 10^8 s^{-1}, the intensity during ramping will remain relatively high (all elastic scattering) and only slowly decrease due to the Debye–Waller factor. If at any temperature the H atom jump frequencies start to exceed 10^8 s^{-1}, either in the same phase or by changing phase, the intensity will start to drop more dramatically as a portion of the purely elastic peak begins to broaden and become quasielastic. As the temperature increases further and if the jump frequency ever exceeds around 10^{10} s^{-1}, the intensity will start to flatten out again because the quasielastic component becomes so broad that its contribution to the total intensity at zero energy transfer becomes negligible.

In Figure 5, all the poly(carba)borate compounds that displayed clear hysteretic transition temperatures between ordered and disordered phases by DSC indicate similar hysteretic behaviors in the anion orientational mobilities. For each of these compounds, there are fairly sharp drops in intensity near the expected phase-transition temperatures upon heating and fairly sharp rises in intensity at the lower hysteretic phase-transition temperatures upon cooling. The differences in the intensity variations vs temperature in the transition regions reflect the temperature-dependent variations in the ordered and disordered phase fractions among the different compounds rather than any changes in the mobilities of a particular phase.[52] These FWS behaviors indicate that the anion jump frequencies are $<10^8$ s^{-1} in the ordered phases near the phase-transition temperature for all the polycarbaborate compounds. The sharp intensity drops observed upon transformations to the disordered phases confirm that the anion jump frequencies are now $>10^{10}$ s^{-1}, although the exact magnitudes cannot be determined without performing quasielastic scans on a different instrument with a broader energy and resolution range.

The FWSs for *a*-$NaB_{11}H_{14}$ in Figure 5 are qualitatively different than the other compounds and reflect the actual progression of anion orientational mobility within the single persistent disordered fcc phase. This is corroborated by the relatively more gradual changes in intensity with temperature

DOI: 10.1021/acs.chemmater.7b04332
Chem. Mater. 2017, 29, 10496–10509

and the lack of any significant thermal hysteresis effects as was observed for the FWSs of other comparable disordered poly(carb)borate compounds.[51,52] In this case, we can say that the orientational jump frequency of the $B_{11}H_{14}^-$ anion in fcc disordered *a*-$NaB_{11}H_{14}$ increases from the order of 10^8 s^{-1} at 230 K to the order of 10^{10} s^{-1} by 320 K.

Besides the FWSs, we also collected a series of complementary QENS spectra on DCS for fcc disordered *a*-$NaB_{11}H_{14}$ at 310, 338, 372, and 410 K; bcc disordered $NaB_{11}H_{14}$ at 372 K; and (*closo*-) $NaCB_{11}H_{12}$ at 370, 400, 438, and 480 K. A spectral fit for *a*-$NaB_{11}H_{14}$ is exemplified in Figure S11 in the Supporting Information. Figure 6 shows the $B_{11}H_{14}^-$ and

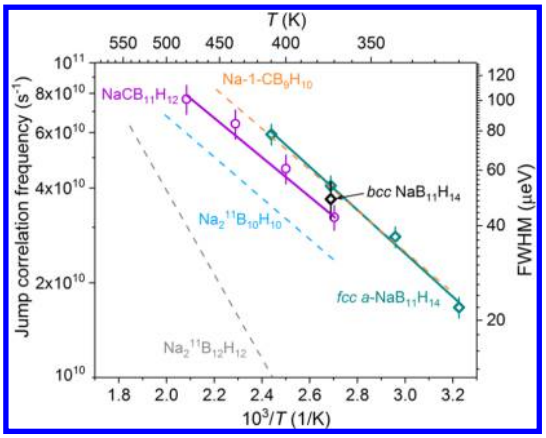

Figure 6. Arrhenius plot of the anion jump correlation frequency vs inverse temperature for disordered *a*-$NaB_{11}H_{14}$, $NaB_{11}H_{14}$, and $NaCB_{11}H_{12}$ in comparison with those for the related sodium *closo*-poly(carba)borate compounds $Na_2{}^{11}B_{12}H_{12}$,[41,51] $Na_2{}^{11}B_{10}H_{10}$,[44] and Na-1-CB_9H_{10}.[44]

$CB_{11}H_{12}^-$ anion jump correlation frequency (τ_1^{-1}) behaviors with temperature for *a*-$NaB_{11}H_{14}$, $NaB_{11}H_{14}$, and $NaCB_{11}H_{12}$, plotted in an Arrhenius fashion. Values were derived from QENS spectra measured at a *Q* value of 0.6 $Å^{-1}$, where the fundamental jump correlation frequency dominates.[44] It is interesting to note that, despite the different fcc disordered *a*-$NaB_{11}H_{14}$ and bcc disordered $NaB_{11}H_{14}$ structures at 372 K, the QENS data indicate similar jump correlation frequencies of ≈4 × 10^{10} s^{-1}, within the current experimental error, although better measurements may well reveal minor differences. Determining why the $B_{11}H_{14}^-$ anions in the two different stacking arrangements possess similar jump frequencies will require comparative molecular dynamics simulations.

The slope of $\ln(\tau_1^{-1})$ vs T^{-1} is $-E_a/k_B$, where E_a is the activation energy for anion reorientation and k_B is the Boltzmann constant. A fit of the data yields respective activation energies of 137(2) and 114(2) meV for *a*-$NaB_{11}H_{14}$ and $NaCB_{11}H_{12}$. The $NaB_{11}H_{14}$ and $NaCB_{11}H_{12}$ jump correlation frequencies and activation energies are compared in Figure 6 with the following related *closo*-poly(carba)borate compounds: $Na_2{}^{11}B_{12}H_{12}$,[41,51] $Na_2{}^{11}B_{10}H_{10}$,[44] and Na-1-CB_9H_{10}.[44] We assume here, to first order, that this fundamental reorientational jump frequency is a relative measure of anion orientational mobilities. Yet, we caution that the situation may be a bit more complicated because the different types of anions may be undergoing somewhat different reorientational mechanisms. The fundamental jump correlation frequency favors the predominant reorientational jump motion within the neutron energy window, which may differ for different anions. Nonetheless, the $B_{11}H_{14}^-$ anion in fcc disordered *a*-$NaB_{11}H_{14}$ interestingly exhibits the highest overall jump correlation frequency (ranging from 1.5 × 10^{10} s^{-1} at 310 K to 6.0 × 10^{10} s^{-1} at 410 K) of all poly(carba)borate anions reported thus far, being very similar to that for 1-$CB_9H_{10}^-$ in hexagonal disordered Na-1-CB_9H_{10}. The $B_{11}H_{14}^-$ jump correlation frequency is about 20−25% higher compared to that for $CB_{11}H_{12}^-$ in fcc disordered $NaCB_{11}H_{12}$. This is consistent with the slightly larger fcc lattice constant (and thus more distance between neighboring anions) observed for *a*-$NaB_{11}H_{14}$ (*a* = 10.1520(19) Å at RT) than for $NaCB_{11}H_{12}$ (*a* = 10.066(3) Å at 356 K).[26] If we compare the RT ordered $NaCB_{11}H_{12}$ unit cell volume per formula unit (950.4 $Å^3$, Z=4)[26] to those for pristine $NaB_{11}H_{14}$ and the other Na *nido*-polycarbaborates from Table 1, it appears that the *nido*-$B_{11}H_{14}^-$ anions do require more volume than the *closo*-$CB_{11}H_{12}^-$ anions, whereas the three different *nido*-polycarbaborate anions require less volume. This may merely be reflecting the likelihood that the $B_{11}H_{14}^-$ anions are already partially orientationally disordered at RT, as suggested by the XRPD results. Anion disorder would tend to require an expanded lattice for accommodation. It is probable that the $B_{11}H_{14}^-$ anions would eventually require comparatively less space than $CB_{11}H_{12}^-$ anions upon formation of a fully ordered $NaB_{11}H_{14}$ at lower temperatures. The 20% larger activation energy observed for the $B_{11}H_{14}^-$ *nido*-anion in *a*-$NaB_{11}H_{14}$ compared to the $CB_{11}H_{12}^-$ *closo*-anion in $NaCB_{11}H_{12}$ may reflect minor average barrier enhancements due to polarization and steric differences associated with hydrogen-rich nest side of the $B_{11}H_{14}^-$ anion.

5. Ionic Conductivities: AC Impedance. Figure 7 compares the temperature dependences of the ionic con-

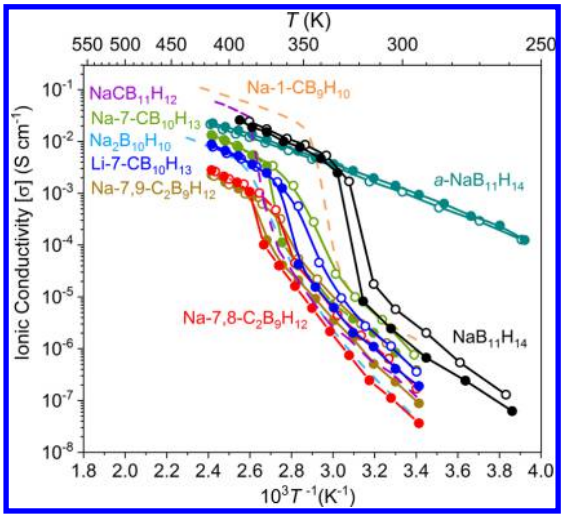

Figure 7. Ionic conductivities versus inverse temperature for all *nido*-compounds during heating (closed circles) and cooling (open circles) segments. Similarly measured conductivities for $NaCB_{11}H_{12}$, Na-1-CB_9H_{10}, and $Na_2B_{10}H_{10}$ upon heating are included for comparison.

ductivities for the various *nido*-compounds as determined by AC impedance measurements upon both heating and cooling. Additional conductivity results upon heating for $NaCB_{11}H_{12}$, Na-1-CB_9H_{10}, and $Na_2B_{10}H_{10}$ reference materials obtained by identical measurement procedures are also shown. The data for all *nido*-compounds show order-of-magnitude or more enhancements in conductivities during heating upon trans-

DOI: 10.1021/acs.chemmater.7b04332
Chem. Mater. 2017, 29, 10496−10509

formation from the ordered phases to the disordered phases. Upon cooling back through the phase transition, there is a reversible hysteretic decrease in the conductivity. As evidenced by XRPD during complementary cycling experiments, the back transformations are often found to be sluggish, as observed for other poly(carba)borate compounds.[24,26,40] A very minor fraction of disordered phase can generally persist below the transition temperature for some period of time (before eventually disappearing). This is manifested in Figure 7 by lower-temperature conductivities during the cooling segment that are somewhat elevated (signaling the presence of some lingering disordered phase) with respect to the values observed at the start of the initial heating segment.

The conductivity behavior for *a*-$NaB_{11}H_{14}$ with temperature is somewhat different, as expected, because it maintains its fcc disordered phase at least down to 30 K, as seen from the corresponding diffraction pattern determined during the QENS measurements. As a result, the conductivity remains relatively high (≈1 mS·cm^{-1} at RT) from an upper temperature of 415 K down to the lowest temperature measured of 255 K with no sudden hysteretic increase or decrease during heating or cooling, respectively.

Using 413 K as a reference temperature, $NaB_{11}H_{14}$ conveys the best ionic conductivity (45 mS·cm^{-1} by extrapolation) among *nido*-compounds, being slightly less than that for $NaCB_{11}H_{12}$ (62 mS·cm^{-1}) and intermediate between that for Na-1-CB_9H_{10} (100 mS·cm^{-1}) and $Na_2B_{10}H_{10}$ (7.0 mS·cm^{-1}). In comparison, the measured ionic conductivities for *a*-$NaB_{11}H_{14}$, Na-7-$CB_{10}H_{13}$, Li-7-$CB_{10}H_{13}$, Na-7,8-$C_2B_9H_{12}$, and Na-7,9-$C_2B_9H_{12}$ at 413 K are 23, 13, 8.7, 2.8, and 2.3 mS·cm^{-1}, respectively. Although the persistent fcc disorder in *a*-$NaB_{11}H_{14}$ allows for superionic conductivity down to subambient temperatures, the 50% lower conductivity for *a*-$NaB_{11}H_{14}$ compared to $NaB_{11}H_{14}$ at 413 K suggests that the presence of impurities incorporated into the former material is an impediment to the cation migration through the lattice. Moreover, it may signal that bcc disorder is a more favorable geometrical arrangement for cationic conduction than fcc disorder, a result that would be consistent with theory.[92]

The conductivities for the disordered phases of the different Na *nido*-compounds seem to trend lower as the lattice volume/formula unit decreases, which makes geometric sense and is consistent with the computed effects of lattice volume on cation conductivity in $Li_2B_{12}H_{12}$.[46,47] Moreover, these downtrending conductivities also seem to correlate with an increase in the number of carbon atoms incorporated into the anion, with over an order of magnitude difference between the best (carbon-free $NaB_{11}H_{14}$) and the worst (dicarbon Na-7,9-$C_2B_9H_{12}$), despite the fact that all of the compounds contain similarly shaped, singly charged anions. Hence, besides cell-volume-correlated differences in interstitial diffusional bottlenecks, a significant portion of the conductivity differences may well be connected to the nontrivial differences in polarizations among the various anions and their effects on the interactions with neighboring cations, which is discussed in more detail in the next section with respect to Mulliken-charge calculations.

We note that the Na^+ conductivity for Na-7-$CB_{10}H_{13}$ is seen to be about 50% higher than the Li^+ conductivity for Li-7-$CB_{10}H_{13}$. This may seem surprising, as the Na^+ cation has a Shannon effective ionic radius (based on 6-fold coordination) of 1.02 Å compared with a corresponding value of only 0.76 Å for Li^+,[93] which could mean lower migration barriers for Li^+ cations within the anionic sublattice. However, there is ample evidence of more facile Na^+ transport in other disordered boron-based anionic compounds, as previously observed for hexagonal disordered Na-1-CB_9H_{10} compared to Li-1-CB_9H_{10}.[27] This is consistent with the slightly smaller unit cell volumes for the Li versions compared to the Na versions of the *closo*- and *nido*-polycarbaborate compounds mentioned.

Conduction activation energies for the disordered *nido*-compound phases as determined from the slope of $\ln(\sigma T)$ vs T^{-1} are 0.321(3), 0.41(2), 0.42(2), 0.39(3), 0.41(3), and 0.49(3) eV for *a*-$NaB_{11}H_{14}$, $NaB_{11}H_{14}$, Na-7-$CB_{10}H_{13}$, Li-7-$CB_{10}H_{13}$, Na-7,8-$C_2B_9H_{12}$, and Na-7,9-$C_2B_9H_{12}$, respectively. These values are within the range of those for disordered $NaCB_{11}H_{12}$ (0.22 eV)[26] and $Na_2B_{10}H_{10}$ (0.47 eV),[25] which also display cubic-close-packed structures, and that for disordered $Na_2B_{12}H_{12}$ (0.21 eV),[24] which possesses a more open, body-centered-cubic structure. The relatively higher activation energies determined for the lower-temperature ordered phases of the latter five respective compounds are 0.61(2), 0.68(3), 0.69(3), 0.78(3), and 0.80(4) eV.

6. Anion Charge Polarizations and Comparisons to *closo*-Compounds. Although the exact values of the charges associated with the anions depend on the atomic charge definition used and on the level of calculation,[94,95] a simple calculation of the Mulliken atomic charge distributions for the various related anions is enough to elucidate qualitative trends in anion polarizations which may, in turn, shed more light on the observed trends in ionic conductivity. Figure 8 illustrates the four different *nido*-anions and two related dodecahydro-

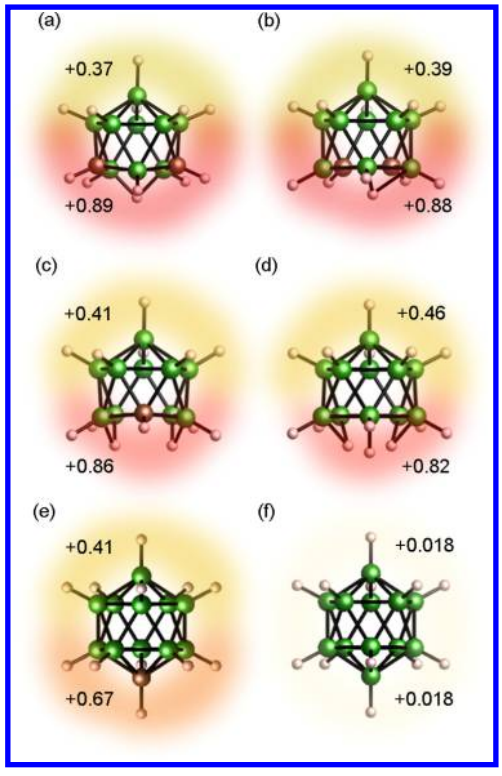

Figure 8. Combined Mulliken charges from DFT calculations for the groupings of H atoms associated with each hemisphere of the different isolated *nido*-anions: (a) 7,9-$C_2B_9H_{12}^-$, (b) 7,8-$C_2B_9H_{12}^-$, (c) 7-$CB_{10}H_{13}^-$, and (d) $B_{11}H_{14}^-$ as well as the related *closo*-anions (e) $CB_{11}H_{12}^-$ and (f) $B_{12}H_{12}^{2-}$ from ref 26. The Mulliken charges for the various B/C skeletal atoms and individual H atoms are not included here but can be found in the .pdf file in the Supporting Information.

DOI: 10.1021/acs.chemmater.7b04332
Chem. Mater. 2017, 29, 10496−10509

closo-dodeca(carba)borate anions, $CB_{11}H_{12}^-$ and $B_{12}H_{12}^{2-}$, with combined Mulliken charges (determined from isolated-anion DFT calculations) for the groupings of H atoms associated with each hemisphere (i.e., top and bottom) of the anions. We note that the number of H atoms on the nest-end hemisphere of the *nido*-anions varies from eight for $B_{11}H_{14}^-$ to seven for 7-$CB_{10}H_{13}^-$ to six for 7,8-$C_2B_9H_{12}^-$ and 7,9-$C_2B_9H_{12}^-$. Figures S1−S4 in the Supporting Information detail the full array of Mulliken charges associated with each individual atom (B, C, or H) of the various anions considered. The atomic charge distribution in *nido*-anions is dominated by the presence of fewer valence electrons than are required for a localized bonding scheme and formation of a cage-like B_{11}, CB_{10}, or C_2B_9 structure. Figure 8 shows the general trend of a more highly polarized arrangement of positive charges on the H atoms of the *nido*-anions compared to the *closo*-anions, with the higher accumulative positive charge situated on the nest-end of the *nido*-anions. Among *nido*-anions, the polarization of hemispherical positive charges is seen to increase with an increase in the number of incorporated C skeletal atoms, the ratios of nest-end:non-nest-end charges being +0.82/+0.46, +0.86/+0.41, +0.88/+0.39, and +0.89/+0.37 for $B_{11}H_{14}^-$, 7-$CB_{10}H_{13}^-$, 7,8-$C_2B_9H_{12}^-$, and 7,9-$C_2B_9H_{12}^-$, respectively. Comparison of the similarly singly charged *closo*-anion, $CB_{11}H_{12}^-$, indicates a significantly less-polarized ratio of +0.67/+0.41.[26] In contrast, the *closo*-anion $B_{12}H_{12}^{2-}$ has a nonpolar ratio of +0.018/+0.018 due to its high icosahedral I_h symmetry.[26] Moreover, the much lower hemispherical charge values are a consequence of its overall double negative charge.

Among the disordered sodium salts of the *nido*-anions and the similarly singly charged *closo*-$CB_{11}H_{12}^-$ anion, there seems to be a good correlation between charge ratio and ionic conductivity, i.e., the compounds with less polarized ratios tend to display higher ionic conductivities. This makes some sense because for the ordered compounds, the more positive ends of the anions in general arrange themselves to avoid the charge-compensating cations.[26,88,94] This behavior likely persists in the disordered superionic salt structures, suggesting that the cation vacancies in the vicinity of the more highly positive end of the anions are not as energetically favorable as conduction hopping sites. This would lead to an overall reduction in the favorable pathways for cation conduction. Having said this, one could also argue that the other less-positive end of the anions would possess more energetically favorable neighboring cation vacancies, which could become the more dominant and facile conduction pathways. Yet, the observed conductivity trends suggest that the best conductivities among the singly charged *nido*- or *closo*-anions derive from the least polarized anions, where all the various conduction pathways are more permissible from an energetics viewpoint. Of course, we point out that, although the $B_{12}H_{12}^{2-}$ anion in Figure 8 has an anomalously low positive charge on its H atom vertices compared to those the other anions mentioned and should lead to the best ionic conductivities, the double charge means that there are twice as many cations required for charge compensation. This necessarily means less available cation vacancies and twice as many blocking cations interfering with conduction. This possibly helps explain the tempered conductivity behavior observed for disordered $Na_2B_{12}H_{12}$, e.g., which is approximately on par with conductivity values for the *nido*-compounds upon extrapolation[24] but actually about an order of magnitude lower than those for $NaCB_{11}H_{12}$.[26]

CONCLUSIONS

We showed that various sodium and lithium *nido*-compounds are promising ionic conductors and exhibit order−disorder phase behaviors similar to those of their *closo*-poly(carba)borate counterparts. Coupling computational simulations and detailed structural characterization provides a fundamental understanding of the factors influencing cation mobility within the interstitial sublattice formed by *nido*-poly(carba)borate anionic cages and reveals a direct correlation between the ionic conductivity, lattice volume, and number of carbon atoms incorporated into the anion. The ionic conductivities for $NaB_{11}H_{14}$, Na-7-$CB_{10}H_{13}$, Li-7-$CB_{10}H_{13}$, Na-7,8-$C_2B_9H_{12}$, and Na-7,9-$C_2B_9H_{12}$ at 413 K are 45, 13, 8.7, 2.8, and 2.3 mS·cm^{-1}, respectively, with conduction activation energies ranging between 0.32 and 0.49 eV. The conductivities for the disordered phases trend lower as the lattice volume/formula unit decreases and number of carbon atoms incorporated into the anion increases. In addition, DFT calculations revealed that charge polarization likely plays an important role on conductivity by affecting the interactions with the alkali metal cations in the crystal lattice. Further experiments are in progress to determine the relative orientational mobilities of the various *nido*-anions in their disordered superionic lattices to ascertain the extent of any possible trends between mobility and conductivity.

Although the superionic conductivities of the various disordered *nido*-compounds investigated here are generally somewhat less than those for the stellar *closo*-compounds Na-1-CB_9H_{10} or $NaCB_{11}H_{12}$, most are as good or better than that for $Na_2B_{10}H_{10}$. Because these *nido*-anions possess similar sizes and arrange in disordered structures that are identical to those for *closo*-poly(carba)borates, it is probable that they can be used to form different mixed-anion solid-solution phases with sub-ambient temperature stabilities. *a*-$NaB_{11}H_{14}$ represents a case in point, where presumably minor unknown impurities are enough to stabilize an fcc disordered structure down to cryogenic temperatures, yielding a respectable 1 mS·cm^{-1} room-temperature ionic conductivity. Although intriguing from a properties viewpoint, it is important as a practical matter to determine the exact origin of this anomalous *a*-$NaB_{11}H_{14}$ behavior via, e.g., controlled doping experiments, which we are currently pursuing. Nonetheless, whether in pure or potentially modified forms, all these *nido*-compounds, including Li versions, significantly expand the available poly(carba)borate compound toolkit for consideration in the design of future tailored multicomponent electrolyte materials.

It is known that the *closo*-polyborate dianions $B_{12}H_{12}^{2-}$ and $B_{10}H_{10}^{2-}$ are the most stable of the polyhedral (carba)borate anions due to their high symmetry and pseudoaromatic bonding. Introducing single carbon substituents into their cage frameworks leads to a favorable unity reduction in negative charge at some cost to thermal stability. Reducing the symmetry further by considering nest-shaped *nido*-anions, as in the present study, enables the retention of the −1 overall charge, which is critical in enabling near-RT superionic conductivity. Opening the closed poly(carba)borate cage could, however, affect the degree of chemical and electrochemical robustness of these *nido*-compounds toward various cathode and anode materials, which would impact their ultimate usefulness as practical solid-electrolyte components of an all-solid-state device. We point out that battery studies involving any of these poly(carba)borate-based electrolytes

DOI: 10.1021/acs.chemmater.7b04332
Chem. Mater. 2017, 29, 10496−10509

have been limited to *closo*-type compounds and generally involved TiS_2 cathodes[26,53,59] (which appear to demonstrate stability toward these electrolytes). We have future plans to test various cathode materials with these *nido*-type compounds to more thoroughly assess their various electrochemical compatibilities.

Finally, a detailed computational mechanistic study is clearly warranted for understanding the chemical and structural factors that yield fast-alkali-ion transport and high electrochemical stability in boron-hydride-anionic compounds, which can accelerate the discovery of practical solid-state ion conductors for energy-storage devices with superior power, rate capability, and safety.

■ ASSOCIATED CONTENT

Supporting Information

The Supporting Information is available free of charge on the ACS Publications website at DOI: 10.1021/acs.chemmater.7b04332.

nido-Anion schematics and Mulliken charges, XRPD model refinements with derived crystallographic parameters, and QENS data (PDF)

Crystallographic information for RT Na-7-$CB_{10}H_{13}$ (CIF)

Crystallographic information for RT Na-7,9-$C_2B_9H_{12}$ (CIF)

DFT-optimized Na-7-$CB_{10}H_{13}$ 0 K gamma-point phonon file (TXT)

DFT-optimized Na-7,8-$C_2B_9H_{12}$ 0 K gamma-point phonon file (TXT)

DFT-optimized Na-7,9-$C_2B_9H_{12}$ 0 K gamma-point phonon file (TXT)

■ AUTHOR INFORMATION

Corresponding Authors

*E-mail: wansi.tang@gmail.com.

*E-mail: mirjana.dimitrievska@nist.gov.

*E-mail: vnstavi@sandia.gov.

ORCID

Mirjana Dimitrievska: 0000-0002-9439-1019

Wei Zhou: 0000-0002-5461-3617

Hui Wu: 0000-0003-0296-5204

A. Alec Talin: 0000-0002-1102-680X

Terrence J. Udovic: 0000-0002-9453-2483

Notes

The authors declare no competing financial interest.

■ ACKNOWLEDGMENTS

M.D. gratefully acknowledges support from the U.S. DOE Office of Energy Efficiency and Renewable Energy, Fuel Cell Technologies Office, under Contract DE-AC36-08GO28308. A.A.T. gratefully acknowledges support from Nanostructures for Electrical Energy Storage (NEES), an Energy Frontier Research Center funded by the U.S. DOE, Office of Science, Office of Basic Energy Sciences, under Award DESC0001160, and the Laboratory Directed Research and Development program. Sandia National Laboratories is a multimission laboratory managed and operated by National Technology and Engineering Solutions of Sandia, LLC, a wholly owned subsidiary of Honeywell International, Inc., for the U.S. Department of Energy's National Nuclear Security Administration under Contract DE-NA-0003525. This work utilized facilities supported in part by the National Science Foundation under Agreement DMR-1508249.

■ REFERENCES

(1) Robinson, A. L.; Janek, J. Solid-State Batteries Enter EV Fray. *MRS Bull.* **2014**, *39*, 1046−1047.

(2) Kim, J. G.; Son, B.; Mukherjee, S.; Schuppert, N.; Bates, A.; Kwon, O.; Choi, M. J.; Chung, H. Y.; Park, S. A Review of Lithium and Non-lithium Based Solid State Batteries. *J. Power Sources* **2015**, *282*, 299−322.

(3) Bachman, J. C.; Muy, S.; Grimaud, A.; Chang, H.; Pour, N.; Lux, S. F.; Paschos, O.; Maglia, F.; Lupart, S.; Lamp, P.; Giordano, L.; Shao-Horn, Y. Inorganic Solid-State Electrolytes for Lithium Batteries: Mechanisms and Properties Governing Ion Conduction. *Chem. Rev.* **2016**, *116*, 140−162.

(4) Stallworth, P. E.; Fontanella, J. J.; Wintersgill, M. C.; Scheidler, C. D.; Immel, J. J.; Greenbaum, S. G.; Gozdz, A. S. NMR, DSC and High Pressure Electrical Conductivity Studies of Liquid and Hybrid Electrolytes. *J. Power Sources* **1999**, *81*−*82*, 739−747.

(5) Ponrouch, A.; Marchante, E.; Courty, M.; Tarascon, J.-M.; Palacın, M. R. In Search of an Optimized Electrolyte for Na-ion Batteries. *Energy Environ. Sci.* **2012**, *5*, 8572−8583.

(6) Kamaya, N.; Homma, K.; Yamakawa, Y.; Hirayama, M.; Kanno, R.; Yonemura, M.; Kamiyama, T.; Kato, Y.; Hama, S.; Kawamoto, K.; Mitsui, A. A Lithium Superionic Conductor. *Nat. Mater.* **2011**, *10*, 682−686.

(7) Seino, M. Y.; Ota, T.; Takada, K.; Hayashi, A.; Tatsumisago, M. A Sulphide Lithium Super Ion Conductor is Superior to Liquid Ion Conductors for Use in Rechargeable Batteries. *Energy Environ. Sci.* **2014**, *7*, 627−631.

(8) Kato, Y.; Hori, S.; Saito, T.; Suzuki, K.; Hirayama, M.; Mitsui, A.; Yonemura, M.; Iba, H.; Kanno, R. High-Power All-Solid-State Batteries using Sulfide Superionic Conductors. *Nat. Energy* **2016**, *1*, 16030.

(9) Zhang, L.; Yang, K.; Mi, J.; Lu, L.; Zhao, L.; Wang, L.; Li, Y.; Zeng, H. Na_3PSe_4: A Novel Chalcogenide Solid Electrolyte with High Ionic Conductivity. *Adv. Energy Mater.* **2015**, *5*, 1501294.

(10) Thangadurai, V.; Narayanan, S.; Pinzaru, D. Garnet-Type Solid-State Fast Li Ion Conductors for Li Batteries: Critical Review. *Chem. Soc. Rev.* **2014**, *43*, 4714−4727.

(11) Thangadurai, V.; Pinzaru, D.; Narayanan, S.; Baral, A. K. Fast Solid-State Li Ion Conducting Garnet-Type Structure Metal Oxides for Energy Storage. *J. Phys. Chem. Lett.* **2015**, *6*, 292−299.

(12) Han, F.; Zhu, Y.; He, X.; Mo, Y.; Wang, C. Electrochemical Stability of $Li_{10}GeP_2S_{12}$ and $Li_7La_3Zr_2O_{12}$ Solid Electrolytes. *Adv. Energy Mater.* **2016**, *6*, 1501590.

(13) Hallinan, D. T., Jr.; Balsara, N. P. Polymer Electrolytes. *Annu. Rev. Mater. Res.* **2013**, *43*, 503−525.

(14) Zhou, W.; Gao, H.; Goodenough, J. B. Low-Cost Hollow Mesoporous Polymer Spheres and All-Solid-State Lithium, Sodium Batteries. *Adv. Energy Mater.* **2016**, *6*, 1501802.

(15) Zhu, Y.; He, X.; Mo, Y. First Principles Study on Electrochemical and Chemical Stability of Solid Electrolyte-Electrode Interfaces in All-Solid-State Li-Ion Batteries. *J. Mater. Chem. A* **2016**, *4*, 3253−3266.

(16) Keen, D. A. Disordering Phenomena in Superionic Conductors. *J. Phys.: Condens. Matter* **2002**, *14*, R819−R857.

(17) Unemoto, A.; Matsuo, M.; Orimo, S. Complex Hydrides for Electrochemical Energy Storage. *Adv. Funct. Mater.* **2014**, *24*, 2267−2279.

(18) Matsuo, M.; Nakamori, Y.; Orimo, S.; Maekawa, H.; Takamura, H. Lithium Superionic Conduction in Lithium Borohydride Accompanied by Structural Transition. *Appl. Phys. Lett.* **2007**, *91*, 224103.

(19) Matsuo, M.; Kuromoto, S.; Sato, T.; Oguchi, H.; Takamura, H.; Orimo, S. Sodium Ionic Conduction in Complex Hydrides with $[BH_4]^-$ and $[NH_2]^-$ Anions. *Appl. Phys. Lett.* **2012**, *100*, 203904.

DOI: 10.1021/acs.chemmater.7b04332
Chem. Mater. 2017, 29, 10496−10509

(20) Teprovich, J. A., Jr.; Colón-Mercado, H. R.; Ward, P. A.; Peters, B.; Giri, S.; Zhou, J.; Greenway, S.; Compton, R. N.; Jena, P.; Zidan, R. Experimental and Theoretical Analysis of Fast Lithium Ionic Conduction in a $LiBH_4$−C_{60} Nanocomposite. *J. Phys. Chem. C* **2014**, *118*, 21755−21761.
(21) Blanchard, D.; Nale, A.; Sveinbjörnsson, D.; Eggenhuisen, T. M.; Verkuijlen, M. H. W.; Suwarno; Vegge, T.; Kentgens, A. P. M.; de Jongh, P. E. Nanoconfined $LiBH_4$ as a Fast Lithium Ion Conductor. *Adv. Funct. Mater.* **2015**, *25*, 184−192.
(22) Unemoto, A.; Wu, H.; Udovic, T. J.; Matsuo, M.; Ikeshoji, T.; Orimo, S. Fast Lithium-Ionic Conduction in a New Complex Hydride−Sulphide Crystalline Phase. *Chem. Commun.* **2016**, *52*, 564−566.
(23) Yan, Y.; Kühnel, R.-S.; Remhof, A.; Duchêne, L.; Cuervo Reyes, E.; Rentsch, D.; Łodziana, Z.; Battaglia, C. A Lithium Amide-Borohydride Solid-State Electrolyte with Lithium-Ion Conductivities Comparable to Liquid Electrolytes. *Adv. Energy Mater.* **2017**, *7*, 1700294.
(24) Udovic, T. J.; Matsuo, M.; Unemoto, A.; Verdal, N.; Stavila, V.; Skripov, A. V.; Rush, J. J.; Takamura, H.; Orimo, S. Sodium Superionic Conduction in $Na_2B_{12}H_{12}$. *Chem. Commun.* **2014**, *50*, 3750−3752.
(25) Udovic, T. J.; Matsuo, M.; Tang, W. S.; Wu, H.; Stavila, V.; Soloninin, A. V.; Skoryunov, R. V.; Babanova, O. A.; Skripov, A. V.; Rush, J. J.; Unemoto, A.; Takamura, H.; Orimo, S. Exceptional Superionic Conductivity in Disordered Sodium Decahydro-*Closo*-Decaborate. *Adv. Mater.* **2014**, *26*, 7622−7626.
(26) Tang, W. S.; Unemoto, A.; Zhou, W.; Stavila, V.; Matsuo, M.; Wu, H.; Orimo, S.; Udovic, T. J. Unparalleled Lithium and Sodium Superionic Conduction in Solid Electrolytes with Large Monovalent Cage-like Anions. *Energy Environ. Sci.* **2015**, *8*, 3637−3645.
(27) Tang, W. S.; Matsuo, M.; Wu, H.; Stavila, V.; Zhou, W.; Talin, A. A.; Soloninin, A. V.; Skoryunov, R. V.; Babanova, O. A.; Skripov, A. V.; Unemoto, A.; Orimo, S.; Udovic, T. J. Liquid-like Ionic Conduction in Solid Lithium and Sodium Monocarba-*Closo*-Decaborates near or at Room Temperature. *Adv. Energy Mater.* **2016**, *6*, 1502237.
(28) Orimo, S.; Nakamori, Y.; Ohba, N.; Miwa, K.; Aoki, M.; Towata, S.; Züttel, A. Experimental Studies on Intermediate Compound of $LiBH_4$. *Appl. Phys. Lett.* **2006**, *89*, 021920.
(29) Hwang, S.-J.; Bowman, R. C.; Reiter, J. W.; Rijssenbeek, J.; Soloveichik, G. L.; Zhao, J.-C.; Kabbour, H.; Ahn, C. C. NMR Confirmation for Formation of $[B_{12}H_{12}]^{2-}$ Complexes during Hydrogen Desorption from Metal Borohydrides. *J. Phys. Chem. C* **2008**, *112*, 3164−3169.
(30) Her, J.-H.; Yousufuddin, M.; Zhou, W.; Jalisatgi, S. S.; Kulleck, J. G.; Zan, J. A.; Hwang, S.-J.; Bowman, R. C., Jr.; Udovic, T. J. Crystal Structure of $Li_2B_{12}H_{12}$: a Possible Intermediate Species in the Decomposition of $LiBH_4$. *Inorg. Chem.* **2008**, *47*, 9757−9759.
(31) Garroni, S.; Milanese, C.; Pottmaier, D.; Mulas, G.; Nolis, P.; Girella, A.; Caputo, R.; Olid, D.; Teixdor, F.; Baricco, M.; Marini, A.; Suriñach, S.; Baró, M. D. Experimental Evidence of $Na_2[B_{12}H_{12}]$ and Na Formation in the Desorption Pathway of the $2NaBH_4 + MgH_2$ System. *J. Phys. Chem. C* **2011**, *115*, 16664−16671.
(32) Pitt, M. P.; Paskevicius, M.; Brown, D. H.; Sheppard, D. A.; Buckley, C. E. Thermal Stability of $Li_2B_{12}H_{12}$ and its Role in the Decomposition of $LiBH_4$. *J. Am. Chem. Soc.* **2013**, *135*, 6930−6941.
(33) White, J. L.; Newhouse, R. J.; Zhang, J. Z.; Udovic, T. J.; Stavila, V. Understanding and Mitigating the Effects of Stable Dodecahydro-*Closo*-Dodecaborate Intermediates on Hydrogen-Storage Reactions. *J. Phys. Chem. C* **2016**, *120*, 25725−25731.
(34) Muetterties, E. L.; Balthis, J. H.; Chia, Y. T.; Knoth, W. H.; Miller, H. C. Chemistry of Boranes. VIII. Salts and Acids of $B_{10}H_{10}^{-2}$ and $B_{12}H_{12}^{-2}$. *Inorg. Chem.* **1964**, *3*, 444−451.
(35) Lu, Z.; Ciucci, F. Metal Borohydrides as Electrolytes for Solid-State Li, Na, Mg, and Ca Batteries: A First-Principles Study. *Chem. Mater.* **2017**, *29*, 9308−9319.
(36) Tubandt, C.; Lorenz, E. Molekularzustand und Elektrisches Leitvermögen Kristallisierter Salze. *Z. Phys. Chem.* **1914**, *87U*, 513−543.
(37) Hull, S. Superionics: Crystal Structures and Conduction Processes. *Rep. Prog. Phys.* **2004**, *67*, 1233−1314.
(38) Wood, B. C.; Marzari, N. Dynamical Structure, Bonding, and Thermodynamics of the Superionic Sublattice in α-AgI. *Phys. Rev. Lett.* **2006**, *97*, 166401.
(39) Skripov, A. V.; Babanova, O. A.; Soloninin, A. V.; Stavila, V.; Verdal, N.; Udovic, T. J.; Rush, J. J. Nuclear Magnetic Resonance Study of Atomic Motion in $A_2B_{12}H_{12}$ (A = Na, K, Rb, Cs): Anion Reorientations and Na^+ Mobility. *J. Phys. Chem. C* **2013**, *117*, 25961−25968.
(40) Verdal, N.; Her, J.-H.; Stavila, V.; Soloninin, A. V.; Babanova, O. A.; Skripov, A. V.; Udovic, T. J.; Rush, J. J. Complex High-Temperature Phase Transitions in $Li_2B_{12}H_{12}$ and $Na_2B_{12}H_{12}$. *J. Solid State Chem.* **2014**, *212*, 81−91.
(41) Verdal, N.; Udovic, T. J.; Stavila, V.; Tang, W. S.; Rush, J. J.; Skripov, A. V. Anion Reorientations in the Superionic Conducting Phase of $Na_2B_{12}H_{12}$. *J. Phys. Chem. C* **2014**, *118*, 17483−17489.
(42) Wu, H.; Tang, W. S.; Stavila, V.; Zhou, W.; Rush, J. J.; Udovic, T. J. The Structural Behavior of $Li_2B_{10}H_{10}$. *J. Phys. Chem. C* **2015**, *119*, 6481−6487.
(43) Skripov, A. V.; Skoryunov, R. V.; Soloninin, A. V.; Babanova, O. A.; Tang, W. S.; Stavila, V.; Udovic, T. J. Anion Reorientations and Cation Diffusion in $LiCB_{11}H_{12}$ and $NaCB_{11}H_{12}$: ^1H, ^7Li, and ^{23}Na NMR Studies. *J. Phys. Chem. C* **2015**, *119*, 26912−26918.
(44) Soloninin, A. V.; Dimitrievska, M.; Skoryunov, R. V.; Babanova, O. A.; Skripov, A. V.; Tang, W. S.; Stavila, V.; Orimo, S.; Udovic, T. J. Comparison of Anion Reorientational Dynamics in MCB_9H_{10} and $M_2B_{10}H_{10}$ (M= Li, Na) via Nuclear Magnetic Resonance and Quasielastic Neutron Scattering Studies. *J. Phys. Chem. C* **2017**, *121*, 1000−1012.
(45) Lu, Z.; Ciucci, F. Structural Origin of the Superionic Na Conduction in $Na_2B_{10}H_{10}$ *Closo*-Borates and Enhanced Conductivity by Na Deficiency for High Performance Solid Electrolytes. *J. Mater. Chem. A* **2016**, *4*, 17740−17748.
(46) Varley, J. B.; Kweon, K.; Mehta, P.; Shea, P.; Heo, T. W.; Udovic, T. J.; Stavila, V.; Wood, B. C. Understanding Ionic Conductivity Trends in Polyborane Solid Electrolytes from Ab Initio Molecular Dynamics. *ACS Energy Lett.* **2017**, *2*, 250−255.
(47) Kweon, K.; Varley, J. B.; Shea, P.; Adelstein, N.; Mehta, P.; Heo, T. W.; Udovic, T. J.; Stavila, V.; Wood, B. C. Structural, Chemical, and Dynamical Frustration: Origins of Superionic Conductivity in *Closo*-borate Solid Electrolytes. *Chem. Mater.* **2017**, *29*, 9142−9153.
(48) Tang, W. S.; Udovic, T. J.; Stavila, V. Altering the Structural Properties of $A_2B_{12}H_{12}$ Compounds via Cation and Anion Modifications. *J. Alloys Compd.* **2015**, *645*, S200−S204.
(49) Bukovsky, E. V.; Peryshkov, D. V.; Wu, H.; Zhou, W.; Tang, W. S.; Jones, W. M.; Stavila, V.; Udovic, T. J.; Strauss, S. H. Comparison of the Coordination of $B_{12}F_{12}^{2-}$, $B_{12}Cl_{12}^{2-}$, and $B_{12}H_{12}^{2-}$ to Na^+ in the Solid State: Crystal Structures and Thermal Behavior of $Na_2B_{12}F_{12}$, $Na_2(H_2O)_4B_{12}F_{12}$, $Na_2B_{12}Cl_{12}$, and $Na_2(H_2O)_6B_{12}Cl_{12}$. *Inorg. Chem.* **2017**, *56*, 4369−4379.
(50) Hansen, B. R. S.; Paskevicius, M.; Jørgensen, M.; Jensen, T. R. Halogenated Sodium-*Closo*-Dodecaboranes as Solid-State Ion Conductors. *Chem. Mater.* **2017**, *29*, 3423−3430.
(51) Tang, W. S.; Matsuo, M.; Wu, H.; Stavila, V.; Unemoto, A.; Orimo, S.; Udovic, T. J. Stabilizing Lithium and Sodium Fast-Ion Conduction in Solid Polyhedral-Borate Salts at Device-Relevant Temperatures. *Energy Storage Mater.* **2016**, *4*, 79−83.
(52) Tang, W. S.; Yoshida, K.; Soloninin, A. V.; Skoryunov, R. V.; Babanova, O. A.; Skripov, A. V.; Dimitrievska, M.; Stavila, V.; Orimo, S.; Udovic, T. J. Stabilizing Superionic-Conducting Structures via Mixed-Anion Solid Solutions of Monocarba-*Closo*-Borate Salts. *ACS Energy Lett.* **2016**, *1*, 659−664.
(53) Yoshida, K.; Sato, T.; Unemoto, A.; Matsuo, M.; Ikeshoji, T.; Udovic, T. J.; Orimo, S. Fast Sodium Ionic Conduction in $Na_2B_{10}H_{10}$-$Na_2B_{12}H_{12}$ Pseudo-Binary Complex Hydride and Application to a Bulk-Type All-Solid-State Battery. *Appl. Phys. Lett.* **2017**, *110*, 103901.
(54) Duchêne, L.; Kühnel, R.-S.; Rentsch, D.; Remhof, A.; Hagemann, H.; Battaglia, C. A Highly Stable Sodium Solid-State

DOI: 10.1021/acs.chemmater.7b04332
Chem. Mater. 2017, 29, 10496−10509

Electrolyte Based on a Dodeca/Deca-borate Equimolar Mixture. *Chem. Commun.* **2017**, *53*, 4195−4198.
(55) Sadikin, Y.; Schouwink, P.; Brighi, M.; Lodziana, Z.; Černý, R. Modified Anion Packing of $Na_2B_{12}H_{12}$ in Close to Room Temperature Superionic Conductors. *Inorg. Chem.* **2017**, *56*, 5006−5016.
(56) He, L.; Li, H.-W.; Hwang, S.-J.; Akiba, E. Facile Solvent-Free Synthesis of Anhydrous Alkali Metal Dodecaborate $M_2B_{12}H_{12}$ (M = Li, Na, K). *J. Phys. Chem. C* **2014**, *118*, 6084−6089.
(57) Teprovich, J. A., Jr.; Colon−Mercado, H.; Washington, A. L., II; Ward, P. A.; Greenway, S.; Missimer, D. M.; Hartman, H.; Velten, J.; Christian, J. H.; Zidan, R. Bi-functional $Li_2B_{12}H_{12}$ for Energy Storage and Conversion Applications: Solid-State Electrolyte and Luminescent Down-Conversion Dye. *J. Mater. Chem. A* **2015**, *3*, 22853−22859.
(58) He, L.; Li, H.-W.; Nakajima, H.; Tumanov, N.; Filinchuk, Y.; Hwang, S.-J.; Sharma, M.; Hagemann, H.; Akiba, E. Synthesis of a Bimetallic Dodecaborate $LiNaB_{12}H_{12}$ with Outstanding Superionic Conductivity. *Chem. Mater.* **2015**, *27*, 5483−5486.
(59) Unemoto, A.; Yoshida, K.; Ikeshoji, T.; Orimo, S. Bulk-Type All-Solid-State Lithium Batteries Using Complex Hydrides Containing Cluster-Anions. *Mater. Trans.* **2016**, *57*, 1639−1644.
(60) Sadikin, Y.; Brighi, M.; Schouwink, P.; Černý, R. Superionic Conduction of Sodium and Lithium in Anion-Mixed Hydroborates $Na_3BH_4B_{12}H_{12}$ and $(Li_{0.7}Na_{0.3})_3BH_4B_{12}H_{12}$. *Adv. Energy Mater.* **2015**, *5*, 1501016.
(61) Paskevicius, M.; Hansen, B. R. S.; Jørgensen, M.; Richter, B.; Jensen, T. R. Multifunctionality of Silver *Closo*-Boranes. *Nat. Commun.* **2017**, *8*, 15136.
(62) Grimes, R. N. *Carboranes*, 3rd ed.; Academic Press: New York, 2016.
(63) Volkov, O.; Dirk, W.; Englert, U.; Paetzold, P. Undecaborates $M_2[B_{11}H_{11}]$: Facile Synthesis, Crystal Structure, and Reactions. *Z. Anorg. Allg. Chem.* **1999**, *625*, 1193−1200.
(64) Kononova, E. G.; Leites, L. A.; Bukalov, S. S.; Pisareva, I. V.; Chizhevsky, I. T.; Kennedy, J. D.; Bould, J. Vibrational Spectrum and Electronic Structure of the $[B_{11}H_{11}]^{2-}$ Dianion. *Eur. J. Inorg. Chem.* **2007**, *31*, 4911−4918.
(65) Moore, E. B., Jr.; Lohr, L. L., Jr.; Lipscomb, W. N. Molecular Orbitals in Some Boron Compounds. *J. Chem. Phys.* **1961**, *35*, 1329−1334.
(66) Aftandilian, V. D.; Miller, H. C.; Parshall, G. W.; Muetterties, E. L. Chemistry of Boranes. V. First Example of a B_{11} Hydride, the $B_{11}H_{14}^-$ Anion. *Inorg. Chem.* **1962**, *1*, 734−737.
(67) Hosmane, N. S.; Wermer, J. R.; Hong, Z.; Getman, T. D.; Shore, S. G. High Yield Preparation of the Tetradecahydroundecaborate(1-) Anion, $[B_{11}H_{14}]^-$, from Pentaborane(9). *Inorg. Chem.* **1987**, *26*, 3638−3639.
(68) Getman, T. D.; Krause, J. A.; Shore, S. G. Synthesis of the New Boron Hydride *Nido*-Undecaborane(15), $B_{11}H_{15}$, and the X-ray Structure of its Conjugate Base Tetradecahydroundecaborate(1-), $[B_{11}H_{14}]^-$. *Inorg. Chem.* **1988**, *27*, 2398−2399.
(69) Maitre, P.; Eisenstein, O.; Michos, D.; Luo, X. L.; Siedle, A. R.; Wisnieski, L.; Zilm, K. W.; Crabtree, R. H. Borate Anion ($B_{11}H_{14}^-$): a Nido Cage with No Hydrogen···Hydrogen Interaction. *J. Am. Chem. Soc.* **1993**, *115*, 7747−7751.
(70) McGrath, T. D.; McGrathand, A. J. $[Ph_3PH][nido\text{-}B_{11}H_{14}]$. *Acta Crystallogr.* **1997**, *CS3*, 229−231.
(71) Whitaker, C. R.; Romerosa, A.; Teixidor, F.; Rius, J. $Cs[CB_{10}H_{13}]$ at 293 K. *Acta Crystallogr., Sect. C: Cryst. Struct. Commun.* **1995**, *CS1*, 188−190.
(72) Romerosa, A. M. Thermal, Structural and Possible Ionic-Conductor Behaviour of $CsB_{10}CH_{13}$ and $CsB_{11}CH_{12}$. *Thermochim. Acta* **1993**, *217*, 123−128.
(73) Davidson, M. G.; Fox, M. A.; Hibbert, T. G.; Howard, J. A. K.; MacKinnon, A.; Neretin, I. S.; Wade, K. Deboronation of *Ortho*-Carborane by an Iminophosphorane: Crystal Structures of the Novel Carborane Adduct $Nido\text{-}C_2B_{10}H_{12}\cdot HNP(NMe_2)_3$ and the Borenium Salt $[(Me_2N)_3PNHBNP(NMe_2)_3]_2O^{2+}(C_2B_9H_{12}^-)_2$. *Chem. Commun.* **1999**, *17*, 1649−1650.
(74) Fox, M. A.; Goeta, A. E.; Howard, J. A. K.; Hughes, A. K.; Johnson, A. L.; Keen, D. A.; Wade, K.; Wilson, C. C. The Molecular Structure of $(PSH^+)(nido\text{-}7,8\text{-}C_2B_9H_{12}^-)$ Determined by Neutron Diffraction (PS = Proton Sponge, 1,8-Bis(dimethylamino)-naphthalene). *Inorg. Chem.* **2001**, *40*, 173−175.
(75) Fox, M. A.; Goeta, A. E.; Hughes, A. K.; Johnson, A. L. Crystal and Molecular Structures of the *Nido*-Carborane Anions, 7,9- and 2,9-$C_2B_9H_{12}^-$. *J. Chem. Soc., Dalton Trans.* **2002**, *10*, 2132−2141.
(76) Rius, J.; Romerosa, A.; Teixidor, F.; Casabó, J.; Miravitlles, C. Phase Transitions in Cesium 7,8-Dicarbaundecaborate(12): A New One-Dimensional Cesium Solid Electrolyte at 210 °C. *Inorg. Chem.* **1991**, *30*, 1376−1379.
(77) The mention of all commercial suppliers in this paper is for clarity and does not imply the recommendation or endorsement of these suppliers by NIST.
(78) Larson, A. C.; Von Dreele, R. B. *General Structure Analysis System*, Report LAUR 86-748; Los Alamos National Laboratory: New Mexico, 1994.
(79) Rodriguez-Carvajal, J. Recent Advances in Magnetic Structure Determination by Neutron Powder Diffraction. *Phys. B* **1993**, *192*, 55−69.
(80) Udovic, T. J.; Brown, C. M.; Leão, J. B.; Brand, P. C.; Jiggetts, R. D.; Zeitoun, R.; Pierce, T. A.; Peral, I.; Copley, J. R. D.; Huang, Q.; Neumann, D. A.; Fields, R. J. The Design of a Bismuth-based Auxiliary Filter for the Removal of Spurious Background Scattering Associated with Filter-Analyzer Neutron Spectrometers. *Nucl. Instrum. Methods Phys. Res., Sect. A* **2008**, *588*, 406−413.
(81) Copley, J. R. D.; Cook, J. C. The Disk Chopper Spectrometer at NIST: A New Instrument for Quasielastic Neutron Scattering Studies. *Chem. Phys.* **2003**, *292*, 477−485.
(82) Meyer, A.; Dimeo, R. M.; Gehring, P. M.; Neumann, D. A. The High Flux Backscattering Spectrometer at the NIST Center for Neutron Research. *Rev. Sci. Instrum.* **2003**, *74*, 2759−2777.
(83) Azuah, R. T.; Kneller, L. R.; Qiu, Y.; Tregenna-Piggott, P. L. W.; Brown, C. M.; Copley, J. R. D.; Dimeo, R. M. DAVE: A Comprehensive Software Suite for the Reduction, Visualization, and Analysis of Low Energy Neutron Spectroscopic Data. *J. Res. Natl. Inst. Stand. Technol.* **2009**, *114*, 341−358.
(84) Giannozzi, P.; Baroni, S.; Bonini, N.; Calandra, M.; Car, R.; Cavazzoni, C.; Ceresoli, D.; Chiarotti, G. L.; Cococcioni, M.; Dabo, I.; Dal Corso, A.; Fabris, S.; Fratesi, G.; de Gironcoli, S.; Gebauer, R.; Gerstmann, U.; Gougoussis, C.; Kokalj, A.; Lazzeri, M.; Martin-Samos, L.; Marzari, N.; Mauri, F.; Mazzarello, R.; Paolini, S.; Pasquarello, A.; Paulatto, L.; Sbraccia, C.; Scandolo, S.; Sclauzero, G.; Seitsonen, A. P.; Smogunov, A.; Umari, P.; Wentzcovitch, R. M. QUANTUM ESPRESSO: A Modular and Open-Source Software Project for Quantum Simulations of Materials. *J. Phys.: Condens. Matter* **2009**, *21*, 395502.
(85) Kresse, G.; Furthmuller, J.; Hafner, J. *Ab initio* Force Constant Approach to Phonon Dispersion Relations of Diamond and Graphite. *Europhys. Lett.* **1995**, *32*, 729−734.
(86) Yildirim, T. Structure and Dynamics from Combined Neutron Scattering and First-Principles Studies. *Chem. Phys.* **2000**, *261*, 205−216.
(87) Momma, K.; Izumi, F. *VESTA* 3 for Three-Dimensional Visualization of Crystal, Volumetric and Morphology Data. *J. Appl. Crystallogr.* **2011**, *44*, 1272−1276.
(88) Wu, H.; Tang, W. S.; Zhou, W.; Tarver, J. D.; Stavila, V.; Brown, C. M.; Udovic, T. J. The Low-Temperature Structural Behavior of Sodium 1-Carba-*Closo*-Decaborate: $NaCB_9H_{10}$. *J. Solid State Chem.* **2016**, *243*, 162−167.
(89) Verdal, N.; Zhou, W.; Stavila, V.; Her, J.-H.; Yousufuddin, M.; Yildirim, T.; Udovic, T. J. *J. Alloys Compd.* **2011**, *509S*, S694−S697.
(90) Wu, H.; Tang, W. S.; Zhou, W.; Stavila, V.; Rush, J. J.; Udovic, T. J. The Structure of Monoclinic $Na_2B_{10}H_{10}$: A Combined Diffraction, Spectroscopy, and Theoretical Approach. *CrystEngComm* **2015**, *17*, 3533−3540.
(91) Phonon animation ascii .txt files in the Supporting Information for the DFT-optimized 0 K ordered polycarbaborate compound

DOI: 10.1021/acs.chemmater.7b04332
Chem. Mater. 2017, 29, 10496−10509

structures can be viewed using the V_Sim software at http://inac.cea.fr/L_Sim/V_Sim/ (accessed December 2017).
(92) Wang, Y.; Richards, W. D.; Ong, S. P.; Miara, L. J.; Kim, J. C.; Mo, Y.; Ceder, G. Design Principles for Solid-State Lithium Superionic Conductors. *Nat. Mater.* **2015**, *14*, 1026−1032.
(93) Shannon, R. D. Revised Effective Ionic Radii and Systematic Studies of Interatomic Distances in Halides and Chalcogenides. *Acta Crystallogr., Sect. A: Cryst. Phys., Diffr., Theor. Gen. Crystallogr.* **1976**, *A32*, 751−767.
(94) Douvris, C.; Michl, J. Update 1 of: Chemistry of the Carba-*Closo*-Dodecaborate(−) Anion, $CB_{11}H_{12}^-$. *Chem. Rev.* **2013**, *113*, PR179−PR233.
(95) Zharov, I.; Weng, T.-C.; Orendt, A. M.; Barich, D. H.; Penner-Hahn, J.; Grant, D. M.; Havlas, Z.; Michl, J. Metal Cation-Methyl Interactions in $CB_{11}Me_{12}^-$ Salts of Me_3Ge^+, Me_3Sn^+, and Me_3Pb^+. *J. Am. Chem. Soc.* **2004**, *126*, 12033−12046.

DOI: 10.1021/acs.chemmater.7b04332
Chem. Mater. 2017, 29, 10496−10509